

540
DC

An Investigation of the Low Temperature Magnetic Transition
in Single Crystal Hematite - ($\alpha\text{-Fe}_2\text{O}_3$)

A Thesis
submitted to the
Faculty of Graduate Studies
University of Manitoba
in partial fulfillment of the
requirements of the degree of

MASTER OF SCIENCE

by

J. Desmond Bean

Winnipeg, Manitoba

September, 1967

ABSTRACT

An Investigation of the Low Temperature Magnetic Transition in Single Crystal Hematite - (α -Fe₂O₃)

By J. Desmond Bean

An extension of a previously known method of computing the temperature dependence of the anisotropy energy in hematite, is used to predict thermodynamically, the Morin transition temperature for a hematite lattice doped with small amounts of aluminum, gallium and titanium.

The effect of a substituted ion on its nearest neighbours is qualitatively examined, and a strong experimental case is made for a change in fine structure anisotropy due to the disruption of superexchange bonds.

The behaviour of a ferrous ion sublattice, produced by titanium doping, is examined for two physical models. The change in transition temperature is calculated, and shown to be in reasonable agreement with earlier data.

Static magnetization measurements were taken over a range of temperature from 20°C. to -190°C. Samples measured were synthetic single crystals of hematite, grown pure, or with up to 2% aluminum or gallium doping, or with up to 0.5% titanium.

Employing a new method, the transition temperature prediction computations allowed the preparation of theoretical magnetization curves of the doped samples, even in the transition region. The above experimental data agreed well with these curves, showing the whole body of the theory has merit experimentally. The inhomogeneity of the doping is shown to be the major factor in the width of the transition.

ACKNOWLEDGEMENTS

The work described in this thesis was carried out at the University of Manitoba during the period from April, 1966 to September, 1967.

The author wishes to express his sincere thanks to Dr C. W. Searle of the Physics Department for his many discussions and helpful suggestions during this work. In addition the author would also thank Dr. A. H. Morrish for the use of the magnetometer and dewar system, and the National Research Council of Canada for the financial support of this project.

TABLE OF CONTENTS

Chapter I

Introduction	1
Crystal Structure of Hematite	3
Sublattice Structure of Hematite	4
Two Sublattice Theory of Canted Antiferromagnetism	9

Chapter II

Calculation of the Total Anisotropy Energy	14
The Effect of Impurity Doping on the Anisotropy Energy	20

Chapter III

Transition Temperature of Titanium Doped Hematite	27
The Fine Structure Energy of Ferrous Ions in Hematite	30
Temperature Dependence of the Ferrous Spin System	33
The Three Sublattice Model of Antiferromagnetism	34
Self-Trapping and Double Exchange	38

Chapter IV

Description of Equipment and Technique.	42
Interpretation of Results	47

Chapter V

Discussion of Results, and Further Proposals	55
--	----

Chapter 1

INTRODUCTION

Hematite has been of continuing interest to investigators of magnetic materials, for over twenty years. This crystalline substance has a strong anisotropic behaviour at normal room temperatures. In addition to antiferromagnetism below the Néel temperature; ($T_n=948^\circ\text{K}$); there also exists a weak spontaneous magnetic moment lying in the (111) crystal plane, for a temperature range between T_n and T_m ; the Morin transition temperature ($T_m=266^\circ\text{K}$). At T_m , the low temperature transition occurs and this weak ferromagnetic moment disappears. Below this temperature the material remains a normal antiferromagnet.

For the experimental study of the low temperature transition, static magnetization measurements were made as a function of both temperature and applied field. Samples employed were synthetic single crystals grown by P. J. Besser and A. H. Morrish at the University of Minnesota. As well as samples grown from spectroscopically pure $\alpha\text{-Fe}_2\text{O}_3$ powders, other crystals measured contained small amounts of contaminants such as titanium, gallium, and aluminum.

A consideration of the free energy of the magnetic spin system provides evidence that the transition is caused by the temperature dependence of the first order anisotropy energy term. Below the transition temperature, the free energy is dominated by an anisotropic energy term which is at a minimum for spins aligned along the [111] direction as antiferromagnetic axis. Above the transition temperature, this same term is of opposite sign; thus favoring spins lying in the (111) plane. At the transition temperature the

anisotropy energy is zero to first order, allowing the spins to flip instantaneously from one preferred direction to the other. Knowledge of the temperature dependence of the anisotropic energy term allows the transition temperature of the pure material to be predicted on a thermodynamic basis. By considering the effects of impurity ions in the crystal and magnetic lattices the change in the temperature dependence of the anisotropic energy can be calculated. Thus the change in transition temperature of doped samples of Hematite can be predicted.

Crystal Structure of Hematite ($\alpha\text{-Fe}_2\text{O}_3$)

$\alpha\text{-Fe}_2\text{O}_3$ has a rhombohedral crystal structure^{1,2} with space group ($R\bar{3}2 = D_{3d}^6$). The crystalline and magnetic unit cells are identical and contain four iron and six oxygen atoms; or two formula units apiece. Each iron atom is surrounded by six oxygen atoms at the corners of a distorted octahedron; with three oxygen atoms closer to the iron than the other three. Figure (1) is a picture of a three dimensional rhombohedral unit cell.

A more suitable symmetry for understanding the magnetic sublattice structure of hematite is given by the hexagonal symmetry² of the hematite lattice when viewed in a projection on the rhombohedral (111) plane. Referring hereafter to the hexagonal symmetry, and hexagonal unit cell, except that the $[\bar{1}11]$ direction and (111) plane refer to the old rhombohedral coordinates, we give a qualitative description of this symmetry as it is shown graphically in figure (2).

Pairs of iron atoms are arranged in lines along the rhombohedral $[\bar{1}11]$ direction; these lines then compose hexagonal columns having hexagonal faces in the rhombohedral (111) plane. Proceeding along any of the six lines of hexagonal symmetry across the columns, each line of iron atoms is shifted one third of the hexagonal unit cell length upwards in relation to the line at the preceding site. A resulting rhombohedral (111) plane of iron atoms will have the iron ions located at the vertices of a network of equilateral triangles; since in the hexagonal symmetry only three of the sites on a hexagon will be occupied at any one

Figure (1)

Hematite Rhombohedral Unit Cell

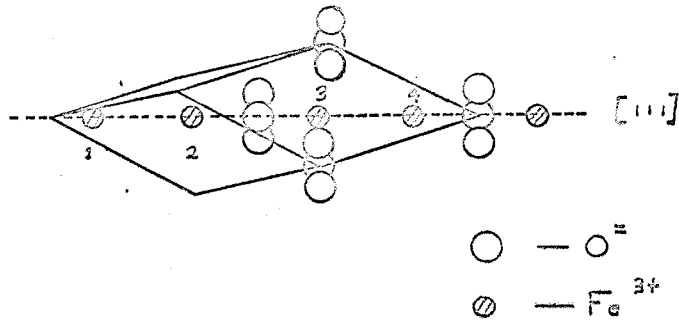
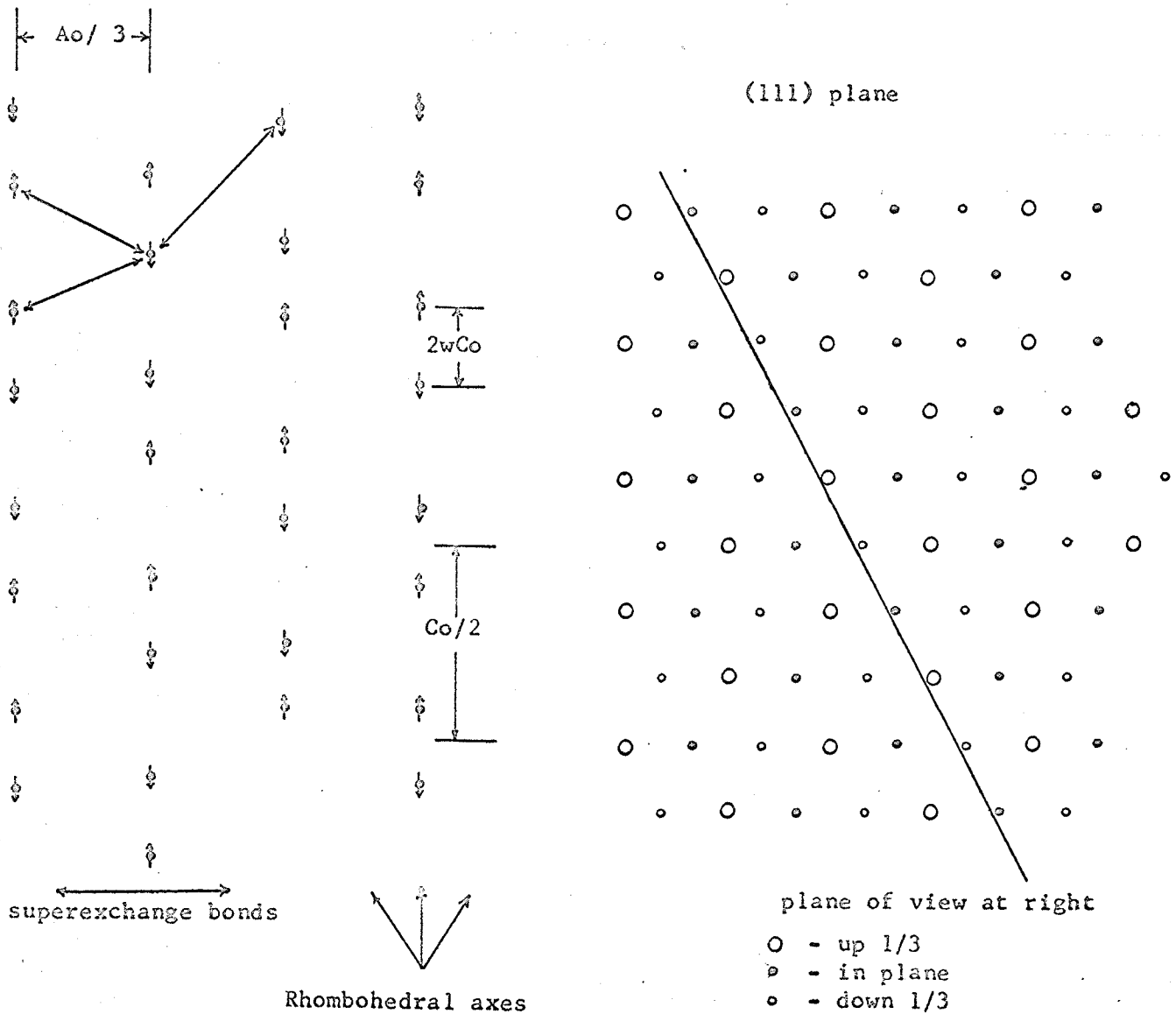


Figure (2)

Hexagonal Magnetic Lattice of Hematite



level. The three other sites will be shifted down one-third cell length; while the centre position will be shifted up one-third. Six of these planes of iron atoms are stacked in layers in the hexagonal unit cell. The octahedra of oxygen atoms positioned about each iron form planes of oxygen atoms lying between the magnetic iron planes. The three important crystal parameters for the magnetic lattice are:

- (1) $a_0=13.749 \text{ \AA}$ Hexagonal Lattice parameter
- (2) $a_0=5.035 \text{ \AA}$ basal plane lattice parameter
- (3) $w=0.1052$ metal ion special position parameter

Sublattice Structure of Hematite

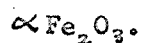
The spin orientations in hematite have been investigated by Shull⁴, and are marked on figure (2) for the antiferromagnetic configuration below the transition temperature. Due to superexchange bonding⁵ through the oxygen atoms, there is an antiferromagnetic interaction between adjacent planes of iron atoms. As a result these form two magnetic sublattices A and B, which will be oppositely aligned along the $[111]$ direction antiferromagnetic axis below the transition temperature.

The classical molecular field formalism^{8,29} will be used in all subsequent calculations. Each magnetic ion of one sublattice lies in a molecular field due to the combined effects of the other sublattice and proportional to that sublattice magnetization. Since there is no evidence that appreciable direct ferromagnetic exchange bonding occurs in Hematite; there is negligible molecular field between ions of the same sublattice.

In this formalism, the effective fields acting on a magnetic ion are due to the isotropic superexchange interaction, anisotropic superexchange interaction, and magnetocrystalline anisotropy.

Considering first the superexchange interaction,^{5,35} a simplified quantum mechanical explanation of its origins was given by Anderson.⁵

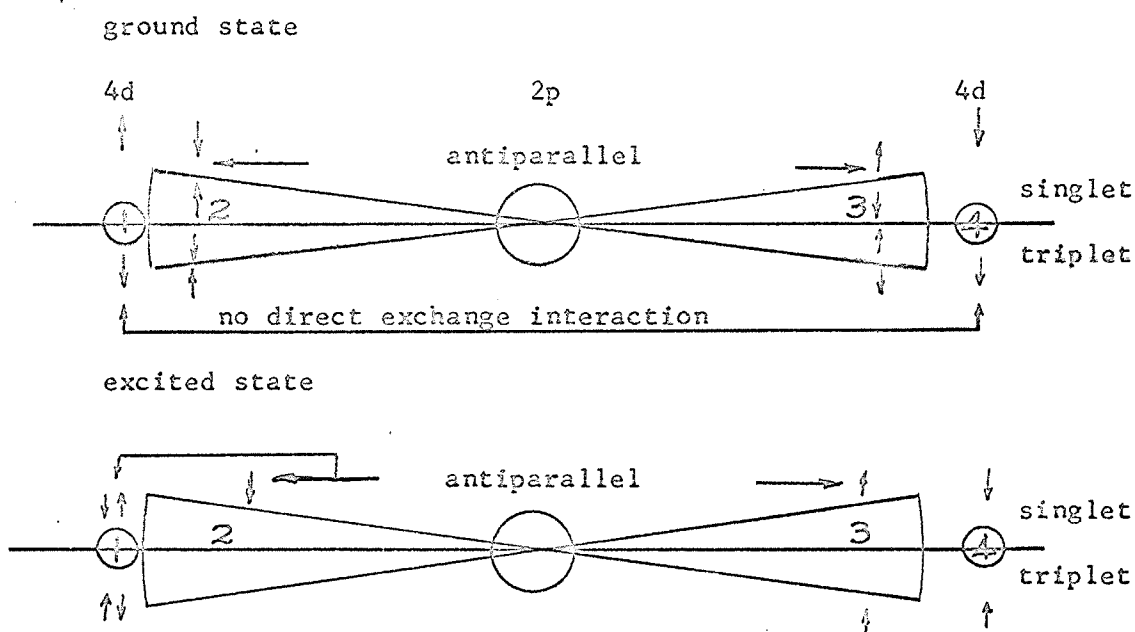
It remains only to note some qualitative features applicable to



The superexchange interaction operates through the $\text{Fe}^{3+} \text{---} \text{O}^{2-} \text{---} \text{Fe}^{3+}$ bonds. While normally there would be no interaction between the two Fe^{3+} next nearest neighbours, since there is no overlap of their electron orbitals, there is a small probability that an electron may be transferred from the oxygen p orbitals to the empty d orbitals on an iron atom. The iron d orbitals are strongly spin coupled antiparallel to the d electrons already on the ion. Transfers of this type give rise to the so called "superexchange" interaction.

If the transfer is viewed as an excited state of a quantum mechanical system; an appreciable exchange integral can arise between the remaining oxygen p electron and the unchanged magnetic atom. Thus the excited states, a singlet and a triplet, will be split as shown in figure (3)

Figure (3) The Indirect Superexchange Interaction



Splitting is possible if a direct exchange interaction exists between 3 and 4.

Since the wave functions are a linear combination of both these states;

$$\Psi = a\Psi_{\text{ground}}^{s,t} + b\Psi_{\text{excited}}^{s,t}$$

and the transition matrix does not mix singlet^(s) and triplet^(t) states, the splitting between the two states will be:

$$(1-1) \quad \Delta E = b^2 (E_s - E_t)_{\text{excited}}$$

or the normal exchange coupling reduced by b^2 . Anderson evaluates this third order perturbation energy to have the form;

$$(1-2) \quad E = \pm \frac{1}{4} b^2 V_{pd} (\underline{S}_1 \cdot \underline{S}_4)$$

where the sign depends on the internal exchange integral between spins 3 and 4. V_{pd} is the matrix element for the transfer of spin 2 to position 1, and b is estimated to be:

$$(1-3) \quad b = \frac{(d | H (\text{unperturbed}) | p)}{\text{Energy of bonding} - \text{Ionic energy}}$$

where H is the unperturbed Hamiltonian of the free ion l .

From this picture of superexchange; geometrical considerations are important for any estimation of the superexchange energy.⁶ Only iron-oxygen-iron bonds, with angles considerably different from 90 degrees and the ions approximately in contact, can be expected to have a large superexchange interaction. Using the method of Gilleo⁶, nine superexchange bonds per iron atom satisfy these conditions and they have been identified on figure (2).

The second of the terms, anisotropic superexchange interaction, was introduced by Moriya,⁷ as an explanation for the weak ferromagnetism found in some antiferromagnetic materials below their Néel temperatures. His more involved calculation in a new formalism produced this result for the interaction between two spins R and R' :

$$(1-4) \quad E_{RR'} = J_{RR'} (\underline{S}(R) \cdot \underline{S}(R')) \\ + \underline{D}_{RR'} \cdot \underline{S}(R) \times \underline{S}(R') \\ + \underline{S}(R) \cdot \underline{\Gamma}_{RR'} \cdot \underline{S}(R')$$

where J , \underline{D} , and $\underline{\Gamma}$ are the isotropic superexchange, the antisymmetric anisotropic spin coupling superexchange, and the symmetric pseudo-dipolar interaction. The magnitude of these terms may be compared by using the relations:

$$(1-5) \quad |\underline{D}| \sim \left(\frac{\Delta g}{g}\right) J, \quad \text{tr}(\underline{\Gamma}) \sim \left(\frac{\Delta g}{g}\right)^2 J.$$

where Δg is the departure of the gyromagnetic ratio from that of a free electron. (approximately 10^{-3} from experimental evidence¹¹ in hematite).

Crystal symmetry will make some components of the antisymmetric coupling matrix vanish; fixing the direction of the Dzialoshinski - Moriya canting vector \underline{D} ,⁴³ related to the analogous quantity from equation (1-4). For the hematite unit cell in figure (1) the midpoint of the second and third iron ions is a center of inversion for the crystal structure. Thus $\underline{D} = 0$ for any interaction between those ions.⁷ For the third and fourth ions however there is no center of inversion, but they lie along the $[111]$ direction, a threefold rotation axis; and therefor \underline{D} is parallel to this axis. There is a direct coupling between the third and fourth ions through two superexchange bonds, but no coupling exists between the second and third ions. Thus the antisymmetric spin coupling interaction vector \underline{D} does point along the $[111]$ direction in hematite.

The third order pseudodipolar term is usually negligible, or can be considered as part of the crystalline anisotropy; as it is identical to the crystalline anisotropy in temperature and angular variations.

The final term affecting the magnetic structure is the crystalline anisotropy energy. For a hexagonal crystal with uniaxial anisotropy in the $[111]$ direction this may be written empirically as a series expansion in $\sin^2 \theta$.

$$(1-6) \quad E_a = \frac{K_1}{2} (\sin^2 \theta_A + \sin^2 \theta_B) + \frac{K_2}{2} (\sin^4 \theta_A + \sin^4 \theta_B) + \dots$$

θ_A and θ_B are the angles between the respective sublattice magnetizations and the easy $[111]$ direction. K_1 and K_2 are the first and second order anisotropy constants respectively, all higher orders are usually neglected. In hematite the energy anisotropy on the (111)

plane is experimentally ^{11,32} four orders of magnitude smaller than the canting energy term, and thus the anisotropy perpendicular to the z axis is virtually zero and the crystal axially symmetric with respect to anisotropy terms. For hematite only K_1 is of the same order as the other terms discussed ³ and thus only it will be included in the free energy calculations. In addition since $\theta_A = -\theta_B$ we may write the simplified anisotropy energy as $E_a = K_1 \sin^2 \theta$; and attribute it to the existence of an effective anisotropy field H_a .

Two Sublattice Theory of Canted Antiferromagnetism

Analogously to the method of standard textbooks^{3,27} the effective field acting on a magnetic dipole (iron ion) is written:

$$(1-7) \quad \underline{H}_{T_e} = \underline{H} + \underline{H}_m + \underline{H}_a + \underline{H}_D$$

where

\underline{H} = applied field

\underline{H}_m = molecular field due to the superexchange interaction and represented as $-\lambda \underline{M}_A$

\underline{H}_a = anisotropy field

\underline{H}_D = canting field due to Dzialoshinski - Moriya interaction which equals $\underline{D} \times \underline{M}_A$

\underline{M}_A = magnetization of one of the magnetic sublattices.

For a dipole of spin angular momentum S there are $(2S+1)$ permissible spin states in the presence of a magnetic field in the direction of quantization. A statistical mechanical calculation of the mean projection of the spin on that axis, for the system at temperature T , yields the familiar

$$m_A = N g \mu_B S B_S(x)$$

$$B_S(x) = \frac{2s+1}{2s} \coth\left(\frac{2s+1}{2s} x\right) - \frac{1}{2s} \coth\left(\frac{x}{2s}\right)$$

$$x = \frac{S g \mu_B H_T}{kT}$$

form of the Brillouin function. (N is the number of ions in the sublattice per c.c., and g, μ_B , k, T, and S have their customary meanings.)

Considering the case below the transition temperature; the anisotropy energy favours the [111] direction as antiferromagnetic axis and the free energy of the individual sublattices becomes:

$$E_A = -H_{TA} \cdot \underline{m}_A = -\frac{1}{2} [2H \cdot \underline{m}_A - \underline{m}_A \cdot \lambda \underline{m}_B]$$

$$E_B = -H_{TB} \cdot \underline{m}_B = -\frac{1}{2} [2H \cdot \underline{m}_B - \underline{m}_B \cdot \lambda \underline{m}_A]$$

The anisotropy energy can be neglected since it is negligible compared to the superexchange energy. From equation (1-8) this gives for the sublattice magnetizations:

$$\underline{m}_A = N_A g \mu_B S B_S \left(\frac{g \mu_B S}{kT} \hat{k} \cdot (H - \lambda \underline{m}_B) \right) \hat{k}$$

$$\underline{m}_B = N_B g \mu_B S B_S \left(\frac{g \mu_B S}{kT} \hat{k} \cdot (H - \lambda \underline{m}_A) \right) \hat{k}$$

where \hat{k} is a unit vector in the direction of quantization.

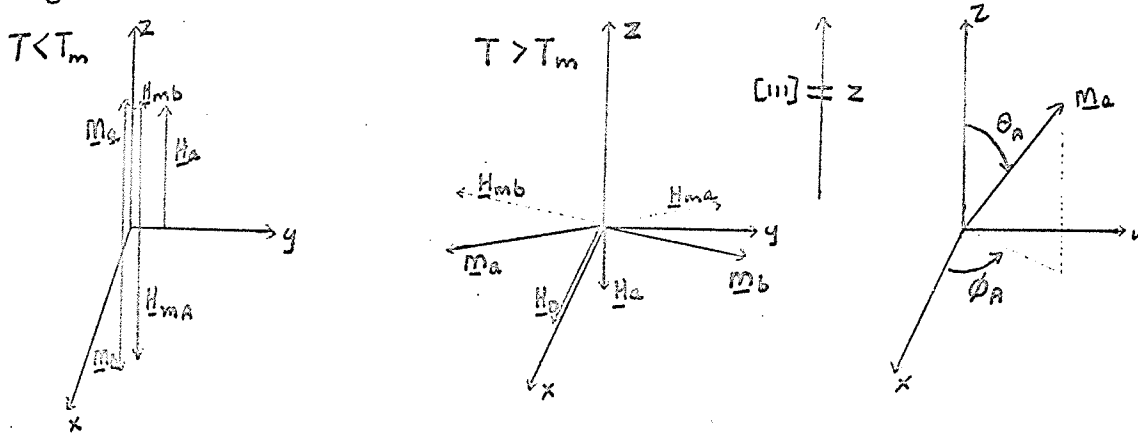
$$\underline{m} = \underline{m}_A + \underline{m}_B \quad N_A = N_B \quad \chi = \left(\frac{\partial \underline{m}}{\partial H} \right)_T$$

The solution of the above equation is difficult except for the limiting conditions.

On raising the temperature upwards to the transition, the field H_a decreases to zero and then changes direction; consequently the sublattice magnetizations now lie in the (111) plane. The free energy term containing H_d is now non zero, although still small compared to the superexchange field. Consequently the amount of

saturation of the sublattice magnetizations is still unchanged under the isotropic superexchange field; but they now lie in the (111) plane, with a small canting from the antiferromagnetic axis due to the action of the canting field. Figure (4) shows the sublattice arrangement for temperatures above and below T_m .

Figure 4.



The free energy is

$$E_T = \lambda (\underline{m}_A \cdot \underline{m}_B) + D \cdot \underline{m}_A \times \underline{m}_B + \frac{k_1}{2} [\sin^2 \theta_A + \sin^2 \theta_B]$$

Rewriting in terms of the defined coordinates

$$E_T = \lambda (m_{Ax} m_{Bx} + m_{Ay} m_{By} + m_{Az} m_{Bz}) + \\ + D (m_{Ax} m_{By} - m_{Ay} m_{Bx}) + \\ + \frac{k_1}{2} [\sin^2 \theta_A + \sin^2 \theta_B]$$

Letting

$$|\underline{m}_A| = |\underline{m}_B| = M$$

This simplifies to:

$$E_T = \lambda M^2 [\sin \theta_A \cos \phi_A \sin \theta_B \cos \phi_B + \sin \theta_A \sin \phi_A \sin \theta_B \sin \phi_B + \\ + \cos \theta_A \cos \theta_B] + D M^2 [\sin \theta_A \cos \phi_A \sin \theta_B \sin \phi_B - \\ - \sin \theta_A \sin \phi_A \sin \theta_B \cos \phi_B] + \frac{k_1}{2} [\sin^2 \theta_A + \sin^2 \theta_B]$$

Since the structure is basically antiferromagnetic, for zero applied fields:

$$\begin{array}{ll} \text{writing} & \text{gives} \\ \theta_A = \theta = \pi - \theta_B & \sin \theta_A = \sin \theta_B = \sin \theta \\ & \cos \theta_B = -\cos \theta \\ \frac{\pi}{2} - \phi_A = \phi = \phi_B - \frac{3\pi}{2} & \cos \phi_A = \cos \phi_B = \sin \phi \\ & \sin \phi_B = -\cos \phi \end{array}$$

Applying these relations (1-13) becomes:

$$(1-14) \quad E_T = -\lambda M^2 [\sin^2 \theta \cos 2\phi - \cos^2 \theta] - DM^2 \sin^2 \theta \sin 2\phi + k_1 \sin^2 \theta$$

To find the torque equation for equilibrium at angle θ :

$$(1-15) \quad \frac{\partial E_T}{\partial \phi} = 0 = -\lambda M^2 \sin^2 \theta 2 \sin 2\phi + DM^2 \sin^2 \theta \cos 2\phi$$

for small $\phi = \phi_0$:

$$(1-16) \quad \phi_0 \approx \frac{D}{2\lambda} = \frac{H_0}{2H_m} \approx \frac{.22 \times 10^5}{1.8 \times 10^7} \approx 1.5 \times 10^{-3}$$

Thus for zero or small external field the sublattice magnetizations are canted in the (111) plane through a small angle ϕ_0 of about 10^{-3} radians, producing a weak spontaneous ferromagnetic moment of;

$$(1-17) \quad |\underline{m}_0| = 2M \sin \phi_0 = \left(\frac{H_0}{2H_m} \right) M$$

with $H_0 = DM$, $H_m = \lambda M$

and

$$(1-18) \quad M = N_A g \mu_B S B_S \left(\frac{S g \mu_B \lambda M}{kT} \right)$$

(1-17) is the expression for the spontaneous magnetization for zero applied field.

From the preceding one can see how the anisotropic free energy affects the orientation of the sublattices. The method above

using equation (1-11), shows that the largest energy term having an angular dependence, is the anisotropy energy k_1 . As the superexchange energy is isotropic, and the canting energy (as evaluated later) small as compared to k_1 , the sublattice orientations which correspond to a minimum in E_T will be determined exclusively by the value of k_1 . Thus by calculating the equilibrium position of the sublattices under the various energy terms, or equivalently, the effective fields applied; $M = m_A + m_B$ can be found.

Chapter 11

Calculation of the Total Anisotropy Energy

The free energy of the hematite sublattice system is given in equations (1-14) and (1-16). The energy terms can be ascribed to the actions of the effective fields H_m , H_a , H_d , and the applied field H . These fields will have orientations as marked on figure (4). Depending on the sign of H_a , the sublattices will have a minimum of the free energy when lying in the basal plane, or lying antiferromagnetically along the $[111]$ direction. For values θ near to 90 degrees, the canting energy due to H_d will also produce a very small effective field in the z direction. This field will also be proven negligible in comparison to the anisotropy field. Since the transition is caused by a reversal in direction of H_a , H_a being the only large field exerting a torque in the x direction, the temperature dependence of H_a was calculated using the method of Artman, Murphy, and Foner³. Although suggested earlier by Kanamori³³, this method was implemented by Artman³ et al. to calculate this temperature dependence and predict the transition temperatures for the pure material.

The two main contributions to the anisotropy energy are:^{9,3} the ordinary dipole-dipole interaction between magnetic ions, and the fine structure anisotropy resulting from higher order spin-orbit coupling interactions with the crystalline field at the ionic site. A much smaller term, the pseudodipolar interaction mentioned earlier, is neglected for the present. The important first order anisotropy constants will be represented as K_{md} , and K_{fs} ; respectively the dipolar and fine structure terms.

Taking an iron atom site as reference point,³ the real magnetic field at that point due to the dipolar interaction with all other ions in the crystal, can be written tensorially as:

$$\underline{H} = \sum_i \underline{D}_i \cdot \mu_i = \underline{D} \cdot \underline{\mu} ; \mu = \sum_i \mu_i$$

where \underline{D} is a tensor; not to be confused with the canting vector \underline{D} ; and μ_i and μ are the magnetic moments of a single ion, and the entire aggregate of ions respectively.

\underline{D} is a tensor depending on the geometry of the lattice, and its elements will reflect the crystal symmetry. In the previously defined coordinates of symmetry \underline{D} will be diagonal with $D_x = D_y = -\frac{1}{2}D_z$, as $D_x + D_y + D_z = 0$ in analogy to the quadrupole problem with the equivalent axial symmetry. The expression for the interaction between dipoles is the familiar;

$$D_z = \mu_p \sum_i \frac{P_i (3 \cos^2 \theta_i - 1)}{r_i^3}$$

and

r_i = distance to dipole i

θ_i = polar angle to dipole i

$P_i = \pm 1$ = orientation of dipole i with respect to the reference dipole

Thus the energy of a dipole μ at an angle θ to the z axis is;

$$\begin{aligned} E &= -\frac{1}{2} \underline{\mu} \cdot \underline{H} \\ &= -\frac{1}{2} \underline{\mu} \cdot \underline{D}' \cdot \underline{\mu} \\ &= -\left[\mu_x^2 D'_{xx} + \mu_y^2 D'_{yy} + \mu_z^2 D'_{zz} \right] \frac{1}{2} \\ &= -\left[(\mu \sin \theta)^2 \frac{D'_z}{2} + (\mu \cos \theta)^2 D'_z \right] \frac{1}{2} \\ &= -\frac{\mu^2}{4} (3 \cos^2 \theta - 1) D'_z \end{aligned}$$

The anisotropy energy is written;

$$E_a = K m d \sin^2 \theta$$

Then

$$(2-4) \quad K_{md} = \frac{+3\mu^2 D_z'}{4} = +\frac{3}{4} S^2 \mu_\beta D_z$$

for definition (2-2) of D_z .

The component D_z was evaluated first by Artman³ and again at this laboratory, with the use of a digital computer. The program summed successive contributions to D_z for surrounding hexagonal columnar shells of ions. After seven lattice spacings, additional contributions changed the value of D_z obtained by less than 0.01%.

With the value of D_z , the anisotropy constant can be calculated from equations (2-3) and (2-4), and the statistical mechanical average of

$$(2-5) \quad K_{md} = \frac{3}{4} N g^2 \mu_\beta^2 \langle S \rangle D_z \langle S \rangle = \frac{3}{4} \mu_\beta^2 N D_z \langle S \rangle^2$$

applying the results from chapter I:

$$(2-6) \quad K_{md} = \frac{3 D_z}{N \mu_\beta^2} M^2 = K_{md}(0) (B_s(x))^2$$

References 8, 9, and 10 have discussed the origin of the single ion anisotropy K_{fs} .³⁶ When an ion is placed in the strong crystalline field existing at a lattice site, the degenerate angular momentum levels of the free ion will be split by large energy intervals. For low temperatures, these energy splittings are so large that virtually all ions will be in the nondegenerate ground state of lowest energy or $\langle L \rangle = 0$. The angular momentum of the system is said to be "quenched".⁸ Through a second order perturbation process, the relativistic spin-orbit coupling, (an interaction between the spin magnetic moment and the orbital and nuclear magnetic fields, represented as $\lambda \underline{L} \cdot \underline{S}$) makes the spin see the crystalline symmetry through the interaction between the orbital angular momentum and the crystalline field. This higher

order effect will occur even with quenched angular momentum and can be thought of as a distortion of the spherical symmetry of the electron cloud.

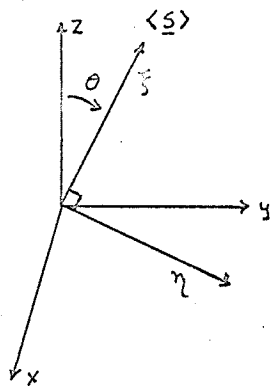
The effect is described phenomenologically^{10, 42} by the spin Hamiltonian in orthorhombic coordinates:

$$(2-7) \quad H = -D_z S_z^2 - D_\xi S_\xi^2 - D_\eta S_\eta^2 - DS_z^2$$

Since the notation D is used for all fine structure splitting terms of this form in the literature, it will be used throughout the following and should not be confused with the two previous D's.

D_z is the only non symmetrical fine structure component in our case of axial symmetry. To find the statistical¹⁰ average of the above energy when the average direction of spins is canted at an angle θ from the z axis the new coordinate system of figure (5^o) is introduced.

Figure (5^o)



z lies in the $\xi\eta$ plane
the ξ axis is along the
average direction of spins.

$$(2-8) \quad -DS_z^2 = -D(\cos\theta S_\xi - \sin\theta S_\eta)^2$$

$$-DS_z^2 = -D[\cos^2\theta S_\xi^2 + \sin^2\theta S_\eta^2 - \sin\theta\cos\theta(S_\eta S_\xi + S_\xi S_\eta)]$$

The ξ axis is the direction of quantization. The average value of DS_z^2 for eigenstate m of S_ξ is given by the equivalent element of the DS_z^2 matrix in the representation in which S_ξ is

diagonal. Therefore the relationships, $(m | S_x^2 | m) = 0$ and;

$$-9) \langle S^2 \rangle = 2\langle S_x^2 \rangle + \langle S_y^2 \rangle + \text{hvs } (m | S_x^2 | m) = \frac{1}{2} (S(S+1)) - \frac{1}{2} m^2$$

Simplifying (2-8) and taking the statistical average yields,

$$-10) -D \langle S_z^2 \rangle = -D \left\{ (\cos^2 \theta - \frac{1}{2} \sin^2 \theta) \langle m^2 \rangle + \frac{1}{2} S(S+1) \sin^2 \theta \right\}$$

$$= -D \left\{ \langle m^2 \rangle + \sin^2 \theta \left(-\frac{3}{2} \langle m^2 \rangle + \frac{1}{2} S(S+1) \right) \right\}$$

where the average value of the magnetic quantum number squared $\langle m^2 \rangle$

is given by:

$$-11) \langle m^2 \rangle = \frac{\sum_{m=-s}^s m^2 e^{\frac{m^2 x}{s}}}{\sum_{m=-s}^s e^{\frac{m^2 x}{s}}} \quad \left(x = \frac{2 |J| z S S_0}{kT} \right)$$

x is the normal argument of the Brillouin function.

The above expression may be evaluated by expanding the following

$$\text{relation: } \frac{d^2}{dx^2} \ln \sum_{m=-s}^s e^{\frac{m^2 x}{s}} = \frac{d}{dx} \frac{\sum_{m=-s}^s \frac{m^2}{s} e^{\frac{m^2 x}{s}}}{\sum_{m=-s}^s e^{\frac{m^2 x}{s}}} =$$

$$= \frac{\sum_{m=-s}^s \left(\frac{m^2}{s}\right)^2 e^{\frac{m^2 x}{s}}}{\sum_{m=-s}^s e^{\frac{m^2 x}{s}}} - \left(\frac{\sum_{m=-s}^s \frac{m^2}{s} e^{\frac{m^2 x}{s}}}{\sum_{m=-s}^s e^{\frac{m^2 x}{s}}} \right)^2$$

Therefore:

$$-12) \frac{1}{s} z \left[\langle m^2 \rangle - \langle m \rangle^2 \right] = \frac{d^2}{dx^2} \ln \sum_{m=-s}^s e^{\frac{m^2 x}{s}}$$

But also expressing this in the form of a sum gives;

$$= e^{-\frac{m^2 x}{s}} = e^{-x} \left[1 + e^{\frac{x}{s}} + \dots + e^{2x} \right] =$$

$$= e^{-x} \left[\frac{1 - e^{\frac{2s+1}{s} x}}{1 - e^{\frac{x}{s}}} \right] = \frac{e^{-x \left(\frac{2s+1}{2s} \right)}}{e^{-\frac{x}{2s}}} \left[\frac{1 - e^{\frac{2s+1}{s} x}}{1 - e^{\frac{x}{s}}} \right] =$$

$$= \frac{\sinh \frac{2s+1}{2s} x}{\sinh \frac{x}{2s}}$$

Differentiating this expression twice gives

$$-13) \frac{d^2}{dx^2} \ln \left[\frac{\sinh \frac{2s+1}{2s} x}{\sinh \frac{x}{2s}} \right] = \frac{d}{dx} B_s(x) =$$

$$= - \left[\left(\frac{2s+1}{2s} \right)^2 \left(1 + \coth^2 \left(\frac{2s+1}{2s} \right) x \right) - \left(\frac{1}{2s} \right)^2 \left(1 + \coth^2 \frac{x}{2s} \right) \right]$$

$$= - \left[\frac{4s(s+1)}{(2s)^2} + \left(\frac{2s+1}{2s} \right)^2 \coth^2 \left(\frac{2s+1}{2s} \right) x - \left(\frac{1}{2s} \right)^2 \coth^2 \frac{x}{2s} \right]$$

Applying equation (2-12) gives

$$\langle m^2 \rangle = \frac{s+1}{s} + \left(\frac{1}{2s}\right)^2 \coth^2 \frac{x}{2s} - \left(\frac{2s+1}{2s}\right)^2 \coth^2 \left(\frac{2s+1}{2s}\right) x + \\ + \left(\frac{2s+1}{2s} \coth \left(\frac{2s+1}{2s}\right) x\right)^2 + \left(\frac{1}{2s} \coth \frac{x}{2s}\right)^2 - 2 \left(\frac{2s+1}{2s}\right) \frac{1}{2s} \coth \left(\frac{2s+1}{2s}\right) x \coth \frac{x}{2s}$$

Simplifying this expression yields

$$\langle m^2 \rangle = s^2 \left[\frac{s+1}{s} - 2 B_s(x) \frac{1}{2s} \coth \frac{x}{2s} \right]$$

substituting this in (2-10) and identifying the anisotropy

energy as $D'fs \sin^2 \theta$ yields

$$D'fs = Ds^2 \left(\frac{s+1}{s} - \frac{3}{2s} B_s(x) \coth \frac{x}{2s} \right)$$

(2-15) expresses the variation of the fine structure anisotropy with temperature.

Summarising the results of the last section:

$$K_{md} = k_{md}(0) (B_s(x))^2 \\ k_{fs} = k_{fs}(0) \left(2(s+1) - 3 B_s(x) \coth \frac{x}{2s} \right) \left(\frac{1}{2s-1} \right)$$

where x is the normal argument of the Brillouin function as determined in equation (1-8) or from the expression involving the Néel temperature from the same simple two sublattice model.

$$x = \frac{3s}{s+1} \frac{T_N}{T} B_s(x)$$

Using these equations and repeating the work of Artman,³ the relations above were evaluated as a function of $\frac{T}{T_N}$. With the computed value of $D_{z,md} = -1.339$ koe. per μ_B per magnetic dipole, K_{md} was calculated as -1.172 cm.^{-1} per magnetic dipole, or an energy density of $92 \times 10^5 \text{ ergs/cm}^3$. To convert this to an effective anisotropy field the energy of this field on a dipole

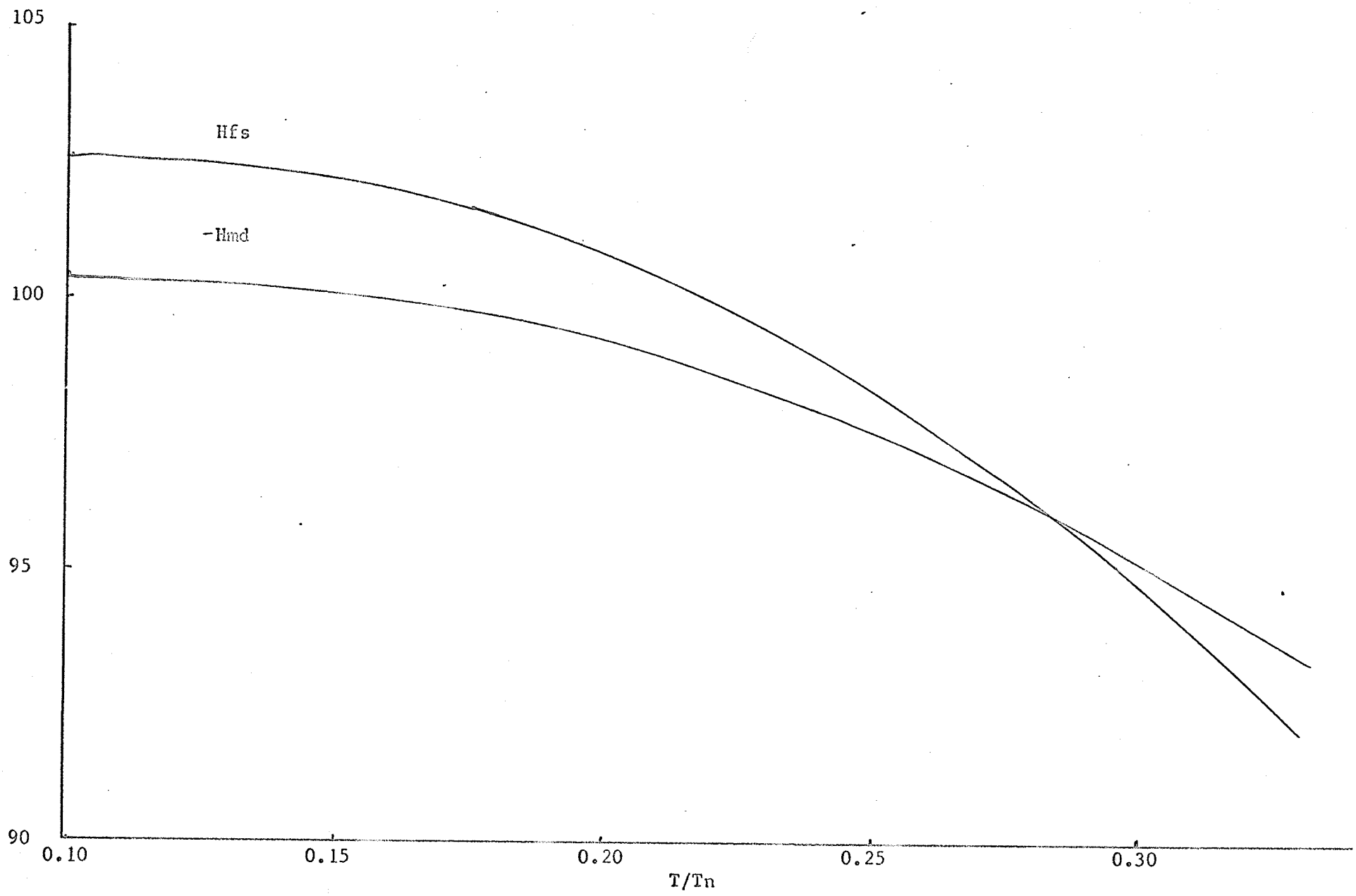
canted off axis by an angle θ is $\chi = K_{md} \sin^2 \theta = -2 H_{md} M \cos \theta$ and solving for equilibrium under the torques when $\theta \approx 0^\circ$ gives $H_{md} = K_{md} / M$, or -100.4×10^2 oe. Besser et al. have found the anisotropy field for pure hematite at liquid nitrogen temperatures to equal $+217$ oe. Since this is equal to the total anisotropy field at absolute zero to a very good approximation, we can evaluate $H_{fs}(0) = H_a(0) - H_{md}(0)$ as 102.6×10^2 oe.^{3,11} Since the fine structure value has not been computed theoretically the experimental value is plotted, along with $-H_{md}$ as a function of the ratio T/T_n in the graph of figure (5). Since the positive H_{fs} is only 2% larger than H_{md} , and decreases more rapidly with increasing T/T_n there is a crossover point at $T_m/T_n = 0.281$ indicating the spins should flip with some characteristic relaxation time, at $T_m = 266^\circ K$;³ a sharp transition is experimentally observed at $T_m = 263^\circ K$. "

The Effect of Impurity Dopings on the Anisotropy Energy

The experiment was performed with single crystals doped with aluminum, gallium, and titanium. This chapter considers the effect of the first two as ions substituted into the hematite lattice. Aluminum and gallium enter the crystal lattice as the ions Al^{3+} and Ga^{3+} with ionic radii 0.51 \AA and 0.62 \AA respectively. It is expected that they will be randomly substituted for Fe^{3+} ions of radius 0.64 \AA , with little or no distortion and strain of the crystal lattice. The substitute ion is treated as a non magnetic site, $S = 0$, undergoing no superexchange interaction.

Effective field $\times 10^2$ oe.

Figure (5)



The effect on K_{md} , letting x be the fraction of ions which are non magnetic, will first cause the decrease of $K_{md}(0)$ by a factor of $(1-x)$ due to the loss of dipolar energy involved in the missing ions. In addition the lack of a magnetic spin in the lattice will reduce the dipolar energies of all other spins depending on their geometrical relationships. The effect of a fraction x of vacancies averaged over all lattice sites will diminish K_{md} by another factor $(1-x)$ since D_z is a linear sum of elements. An alternate method of proving this last point is to see that adding an oppositely directed spin to a lattice site of the pure crystal gives the effect of a substituted ion. This spin will have energy $-D_z$ and will be a positive contribution, decreasing the negative value of K_{md} . These two effects give K_{md} a quadratic dependence on doping.

$$K_{md}(0) = K_{md}(0) (1 - x)$$

A much smaller effect is also included in the calculations. For the nine next nearest neighbours of a substituted ion; those normally having a superexchange bond; it can be expected that the argument of its Brillouin function would be reduced due to the loss of the superexchange interaction. In effect the molecular field on this ion will be smaller, and its orientation along the direction of quantization less rigid. The temperature dependence of its average spin orientation will be decreased. From (2-5) the new temperature dependence of this dipolar term is:

$$K_{md}'(0) = K_{md}(0) B_s(x) B_s\left(\frac{9}{7}x\right)$$

Calculations show that since these nearest neighbours lie beside a substitute ion their individual dipolar energies at $T = 0^\circ\text{K}$ are

smaller than normal, in addition to the changed temperature dependence. Using equation (2-2) the corrections are calculated in the computer program.

The effect of the substitution on the fine structure energy will diminish it also by the factor $(1 - x)$, which subtracts the contribution of those ions having no magnetic interaction. By the same argument as given previously the nine nearest neighbours will have a decreased argument of the Brillouin function due to the loss of superexchange bond energy. The temperature dependence of the fine structure anisotropy for the nine ions will decrease more rapidly than that of the unaffected ones.

Finally, the substitution of non magnetic ions can be expected to change $K_f(0)$ for many of the nearest neighbours to the substitution center. These fine structure energies will have two origins, the pseudodipolar interaction, and the second order spin orbit-coupling to the crystalline field. The latter, much larger term is believed physically to be a distortion of the ferric ion 3d electron shell from spherical symmetry. M. H. L. Pryce¹² has shown by perturbation calculations that a second order process in the spin-spin interaction, and z axis crystalline field component $V = H(2z^2 - x^2 - y^2)$ leads to a term in the Spin Hamiltonian of $-DSz^2$. Calculation of the constant D shows that it is linearly dependent on $H'/\Delta E$ where ΔE is the energy between the 3d and 4s levels of a free ion. The crystalline field in the z direction will be due to the distorted octahedron of oxygen

atoms about each iron; and possibly the nearest iron ion paired to that substitution center. If the substitutional ion were not as spherically symmetric, or of the same size as the iron atom it replaced, the other iron atom of the pair would see a greatly changed crystalline field, and thus a greatly changed fine structure.

However, the ions Al^{3+} and Ga^{3+} have closed nondegenerate 3p and 3d shells respectively. As such they are spherically symmetric and less than or equal to the ferric ions in size. Thus no change in crystalline field, or even in the radial electron probability integrals entering into the relation for D_z , can be expected. Estimates of the magnitude of the D_z term obtained from Pryce's formula give values an order of magnitude less than the experimental values in hematite. Since the pseudodipolar term is small by all estimates^{9, 16} there must be some other origin for the interaction represented by D_z .

That some such change is occurring is supported by measurements in Al_2O_3 (corundum or sapphire) dilutely doped with ferric ions.¹³ The fine structure anisotropy term D_z measured in this substance by E. P. R. methods is -1.4 times the antiferromagnetic value. Since the two lattices are identical, it is evident that the fine structure anisotropy should change sign on changing from the antiferromagnetic ordering to the paramagnetic disordering above the Néel temperature. Recent papers^{14, 15, 24, 27} expand on the work of Pryce to introduce: mixing of excited states in the crystalline field, overlap of the oxygen orbitals

in the s shell, and other anisotropic covalent effects such as charge transfer from the ligand ion. The calculations of the second paper¹⁵ show that contributions to Dz arise from all these mechanisms, and oppose each other in sign. The estimates for covalency have the same sign as the antiferromagnetic value of Kfs. If the superexchange energy represents a strong covalent bond, with its associated anisotropic covalency, the loss of that bond, as in the case of substituting a non magnetic ion, would allow other crystalline field anisotropies to predominate and change the sign of the anisotropy energy. This effect occurring over nine ions, will be equivalent to a new fine structure energy Kfs' for one ferric nearest neighbour of;

$$\frac{Kfs'}{Kfs} = \frac{Kfs}{Kfs} + \left(\frac{9 \text{ nearest neighbours}}{\text{total no. of bonds}} \right) \frac{(\text{total no. of changed bonds/ion}) Kfs''}{Kfs}$$

where Kfs'' is the EPR value in the paramagnetic region and:

$$(2-18) \quad \frac{Kfs'}{Kfs} = 1 + 9\left(\frac{1}{9}\right)(-1.4) = -0.4$$

Using the corrections derived earlier, for changes in Hmd and Hfs with doping, the sum of these fields is equated at T = 0°K to the total anisotropy fields measured by Besser et al. The difference between the experimental anisotropy field, and the corrected theoretical one is due to an effect like (2-18). Thus;

$$Hmd + Hfs = Hk = (100.4)(1-2x) - (102.6)(1-2x) - (102.6) \times \left(\frac{Kfs'}{Kfs} \right)$$

where Hk is the total anisotropy field at T = 0°K. The experimental ratio Kfs'/Kfs can thus be found from equation (2-19) as a

comparison to the results of (2-18).

$$(2-19) \quad \frac{Kfs'(0)}{Kfs(0)} = \frac{100.4(1-2x) + Hk \times 10^{-2} - 102.6(1-2x)}{102.6(x)}$$

where x = atomic fraction of doping ions, T = 0°K

Table I shows this fraction as a function of doping and substitute

ion.

Table I

$\frac{Kfs^?}{Kfs}$	Theoretical ratio	% atomic doping	doping material
-0.41	-0.4	0.3	Ga ³⁺
-0.49	-0.4	0.6	"
-0.41	-0.4	1.38	"
-0.25	-0.4	0.423	Al ³⁺
-0.27	-0.4	0.826	"
-0.25	-0.4	1.276	"
-0.25	-0.4	2.06	"

For Al³⁺ the fraction can range from + 1 in the undoped case to - 1.4 for the dilute case. The experimental ratio -0.25 is an accurate constant for all four doping cases. This will be strong support for some process involving the individual superexchange bonds. Also since the fraction does not change with doping, there may be no large variation of doping throughout the crystal so that very few ferric ions have more than one broken superexchange bond apiece. For these circumstances, the model examined previously will hold, and it is supported by the experimental evidence. To apply the same idea to other anisotropy energies would be fruitless, as they are too small. For example, the pseudodipolar term, on the order of $\frac{4g}{9}Hd$ or ≈ 50 oe. (equation (1-5)), would have to change by a factor of -250. The anisotropy of the ferric ion necessary would be $\frac{4g}{9} = 0.015$ instead of 10^{-3} , and the resulting increase in canting field (15% change for 1% doping), would be easily detectable; if indeed equation (1-5) has any meaning in such a case when the symmetry producing the canting field has changed. However no change of canting field with doping appears in our measurements.

Figure (6) reproduces the computer program which calculates values of $B_s(x)$, H_{md} , and H_{fs} as functions of T/T_n , and percentage doping.

Figure (7) shows typical curves obtained in the case of one particular doping.

In figure (7)

H_{md}	~	Dipole-dipole field	
H_{fs}	~	Fine structure field	$\frac{K_{fs}'}{K_{fs}} = -0.25$
H_{fs}'	~	Fine structure field	$\frac{K_{fs}''}{K_{fs}} = -1.4$
H_{fs}''	~	Fine structure field	$\frac{K_{fs}'''}{K_{fs}} = +1.0$

Table II is a comparison of the transition temperatures predicted by our calculations, with transition temperatures measured by Besser, Morrish, and Searle; and reported in reference 11.

Table II

Doping percentage	T/T_n	T_m (predicted) °K	T_m (11) °K
Pure	0.281	266	263
0.30% Ga	0.274	259	257 - 258
0.60%	0.268	254	251 - 253
1.38%	0.249	237	241 - 245
0.423% Al	0.275	260	258
0.826%	0.270	255	255 - 256
1.276%	0.262	248	252
2.06%	0.249	236	242 - 254

Figure (6) Computer Program for Aluminum and Gallium Doped Crystals

```

24 READ(1,25) DOPE,FACT
25 FORMAT(3(6X,E6.3))
   S=2.5
   WRITE(3,21) S
   XB=1.0
   TNT=.05
   BSX=1.0
1 CONTINUE
   X=(3*S)*BSX/(TNT*(S.1))
   BSX=(2*S+1)/(2*S*TANH((2*S.1)*X/(2*S)))-1/(2*S*TANH(X/(2*S)))
   TEST=ABS((X-XB)/X)
   XB=X
   IF(TEST-.00001)22,1,1
22 CONTINUE
   BSX1=BSX
   BSM1=(2*(S.1)-3*BSX/TANH(X/(2*S)))/(2*S-1)*102.6
   BSM2=BSX*BSX*100.4
   BSM3=BSM1
   X=X*.88889
   BSX=(2*S+1)/(2*S*TANH((2*S.1)*X/(2*S)))-1/(2*S*TANH(X/(2*S)))
   BSM1=(2*(S.1)-3*BSX/TANH(X/(2*S)))/(2*S-1)*102.6
   BSM9=(1-10*DOPE)*BSM3+9*DOPE*BSM1
   BSM4=(1-12.4*DOPE)*BSM3+9*DOPE*BSM1
   BSM1=(1-(10+FACT)*DOPE)*BSM3+9*DOPE*BSM1
   BSM6=BSM2
   BSM5=881.32*DOPE*BSX*BSX1
   BSM7=925.82*DOPE*BSX*BSX1
   BSM8=BSM7+(1-11.112*DOPE)*BSM6
   BSM2=BSM5+(1-10.778*DOPE)*BSM6
   WRITE(3,20) TNT,BSX1,BSM8,BSM4,BSM5,BSM6
   WRITE(3,20) TNT,X,BSM9,BSM1,BSM2,DOPE
20 FORMAT(1H ,2X,F3.2,5(10X,E12.6))
21 FORMAT(1H1,6HFOR S=,F4.1,40H TEMPERATURE DEPENDENCE OF ANISTROPY
11S//1H ,2X,4HTN/T,12X,8HARGUMENT,14X,8HBS(ARG.),14X,4HXKFS,18X,4H
2XKMD)
   TNT=TNT+.01
   IF(TNT-.40)1,1,23
23 CONTINUE
   GO TO 24
END

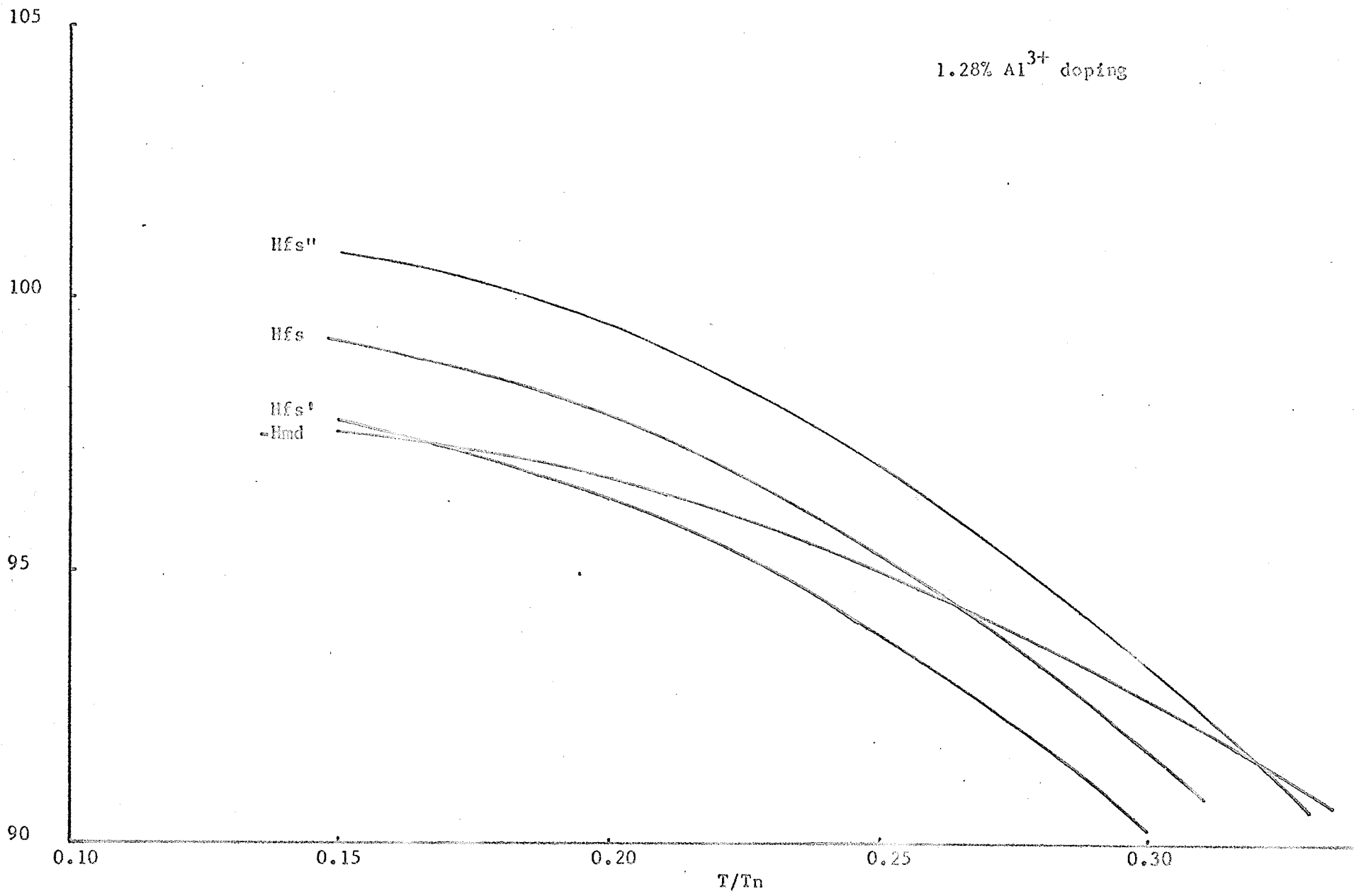
```

Effective Anisotropy Fields for Aluminum Doped Hematite

Figure (7)

Effective field - $\infty \cdot 10^2$

1.28% Al^{3+} doping



Chapter III

Transition Temperatures of Titanium Doped Hematite

When synthetic single crystals of hematite are doped with Ti^{4+} ions there is a much larger shift of transition temperature with doping than was observed earlier with aluminum and gallium doped crystals. Doping of more than 0.25% suppress the transition completely, and no crystals have yet been grown with more than 0.5% atomic doping of titanium.

This effect is caused by the production of Fe^{2+} ions in the lattice, to balance the excess charge on the titanium substitute ions. The titanium ions in the lattice essentially donate electrons to conduction bands of the lattice, and these electrons will move through the lattice hopping from ferric ion to ferric ion. Measurements of the time required to hop from one ion to another show that this is a very small quantity $\approx 10^{-12}$ seconds³². Crude calculations from the conductivity results,³² presuming the electrons to hop in the direction of applied field when not self-trapped on an ion, give an average time on a ferric ion of 10^{-5} seconds. This is supported by the data of reference 38 showing a large effective mass for the mobile electron. When the time spent on an ion greatly exceeds the amount of time spent hopping, the effect is essentially that of x atomic percent ferrous ions randomly placed in the hematite lattice; where x is the percentage titanium doping. The method used in this section will be to introduce new effects due to the x percent Fe^{2+} ions; along with the changes due to the x percent Ti^{4+} ions treated in the manner of the previous chapter.

The ferrous ions have a smaller spin quantum number $S = 2$, and thus will have a smaller dipole-dipole energy as calculated from the results of chapter II. The temperature dependence of the ferrous saturation in the molecular field will follow $B_2(x')$, where the value of the argument x' depends on the sublattice interactions with the ferrous ions, and is calculated later for two reasonable physical models.

The fine structure temperature dependence will also change for $S = 2$. Since the degenerate ground state of the free ion has $L = 2$, there is a possibility of first order spin-orbit coupling, and a resultant large anisotropy in the crystalline field.

The effective fine structure anisotropy field at the ferrous ions can be calculated by the method used previously, from the data of Besser et al.¹¹ Following the arguments of the previous chapter, the titanium ion is presumed to cause the anisotropy of one ferric ion to change to a value $\frac{Kfs''(0)}{Kfs(0)} = -0.40$; as the size and symmetry of the titanium ions are close to those of the gallium. The formula used becomes:

(3-1)

$$\frac{Kfs''(0)}{Kfs(0)} = \frac{100.4(1-2.36x) + Hk \times 10^{-2} - (1-2x)102.6 + 42.1(x)}{102.6(x)}$$

when $x =$ atomic fraction of doping, $42.1(x) =$ new Kfs' of Ti^{4+} nearest neighbour

$Hk =$ anisotropy field at $77^\circ K.$, $0.36x =$ dipolar energy loss of Fe^{2+} ions

In the two cases for which anisotropy fields have been measured:

$$x = 0.00045 \quad \frac{Kfs''}{Kfs} = -4.83 \quad Hfs = 5.0 \times 10^4 \text{ oe.}$$

$$Hk = 197 \text{ oe.}$$

$$x = 0.00081 \quad \frac{Kfs''}{Kfs} = -8.22 \quad Hfs = 8.4 \times 10^5 \text{ oe.}$$

$$Hk = 151 \text{ oe.}$$

Since these values change greatly with increase in doping, it indicates that the doping with titanium is possibly not uniform throughout

the crystal and possibly that the titanium atoms have a preference to group on planes, as in the illmenite-hematite system.

Using these values of anisotropy fields the new values H_{fs} and H_{md} were calculated by the program of figure (8). Table III shows transition temperatures predicted by this program for several different ratios of K''/K as well as values given in reference 11.

Table III

Titanium doping	K''/K	T_m (calc.)	Transition temperature (11)
0.045%	-4.83	260 ° K.	252 - 264 ° K.
	-8.22	254	
0.081%	-4.83	256	239 - 253
	-8.22	242	
0.170%	-4.83	250	206 - 246
	-8.22	212	
	-9.25	201	
0.258%	suppressed for $\frac{K''}{K} < -9$		transition is suppressed
0.353%	suppressed for $\frac{K''}{K} < -6$		to less than 12°K.

Figure (9) shows H_{fs} and H_{md} curves for a selected titanium doping as the value of K''/K is varied.

From this description of these calculations there can be no accurate statement about the value of K_{fs}''/K_{fs} as a function of doping. The value around -9 gives the best fit to the experimental data, and it has been used in all ensuing calculations. In the calculations for transition

temperature the argument x in the fine structure dependence is calculated for the action of a single sublattice molecular field in the direction of average spin. This is essentially the first model discussed below. Any interaction between the ferrous ions which increased with increased doping, would cause a change in the amount of anisotropy energy needed to fit the $T = 0^\circ$ K conditions; in effect the value of K''/K would change. In the ensuing paragraphs it is shown how energies of this order can be expected from ferrous ions in the crystalline field of hematite.

The Fine Structure Energy of Ferrous Ions in Hematite

The ferrous ions produced for charge balance in titanium doped hematite will have the degenerate free electron groundstate split into levels in the crystalline field.¹⁶ The ferrous ion will have six d electrons; of which five will fill up the plus spin levels, and the sixth will go in the lowest energy state remaining. Using a qualitative argument similar to that of Chikazumi⁸ and Anderson¹⁶ to predict the ground state of the system, the distorted octahedron of oxygen ions will set up a strong uniaxial electric field along the z axis; the $[111]$ direction. Spatial probability plots of the five d orbitals show that for the $[111]$ direction as axis of quantization, the three d orbitals will extend outwards in the direction of the negatively charged oxygen ions.⁸ Physically, these orbitals should be higher in energy due to the repulsion of the negative electron clouds. The triplet and doublet states, according to reference 16, should be split by energy interval $10 Dq$ ¹⁶ (center of gravity constant), a factor²³ of 10^4 cm.^{-1} for the ferrous ion in similar sites. The extra electron will lie in an admixture of the

$d\gamma$ orbitals ($2z^2-x^2-y^2$) extending along the z axis, and (x^2-y^2) spread in the basal plane. Since the nearest neighbour iron ion of the pair lies on the z axis, attraction from the positive ferric ion should make the ($2z^2-x^2-y^2$) orbital lower in energy. For low temperatures the ground state will be almost nondegenerate. Therefore $\langle L \rangle \approx 0$ and only small first order anisotropies will exist in the quenched angular momentum state. While this term cannot be estimated, its angular dependence would be $\langle L \rangle \langle S \rangle |\cos \theta|$ (θ being the polar angle) and its effect on the transition temperature would be completely different from that of K_{nd} and K_{fs} . However for strong uniaxial fields, experimental evidence shows that the above argument holds in general, and angular momentum is always quenched by the crystalline field^{16,17,21}.

The second order perturbation of the spin-orbit interaction on the Hamiltonian of the ferrous ion is the fine structure term in the spin Hamiltonian. A literature search was instigated to find estimates of the spin-orbit interaction in similar sites. In general the order of magnitude of anisotropy in the cubic crystalline symmetry of ferrites (on which most measurements are made) is far smaller than the case of strong uniaxial symmetry. To evaluate anisotropy energy from the spin Hamiltonian anisotropy term $-DSz^2$, relation (2-15) is evaluated at $T = 0^\circ K$.

$$(3-2) \quad \frac{1}{2} k_{ss} \sin^2 \theta = -D S^2 \left(\frac{S+1}{S} - \frac{3}{2S} \right) \sin^2 \theta$$

or for the case of $S = 2$ and a single ion:

$$K_{fs} = -6D \quad \text{or} \quad K_{fs} = 6ND$$

N = the number of ferrous ions per cubic centimeter.

Table IV shows values of K_{fs} for the most similar structures found.

Table IV

Material	Crystal Structure	Ref.	Remarks, Quantity, and units
Fe_3O_4	spinel	20	$K_1 = -2.0 \times 10^5 \text{ erg/c.c.}$
NiFe_2O_4	"	19	$K_1 = -1.18 \times 10^5 \text{ erg/c.c.}$
Fe_3O_4	"	42	$K_1 = +3.56 \times 10^{-2} \text{ cm}^{-1} / \text{Fe}^{2+} \text{ ion}$
FeF_2	rutile	28	$K_{fs} = 7.3 \text{ cm}^{-1} / \text{Fe}^{2+} \text{ ion}$
FeF_2	"	17	$K_{fs} = 10.5 \text{ cm}^{-1} / \text{Fe}^{2+} \text{ ion}$
$\alpha\text{-Fe}_2\text{O}_3$	corundum	11	$K_{fs} = 1.2 \text{ cm}^{-1} / \text{Fe}^{3+} \text{ ion}$ 9.0
Al_2O_3	"	13	$K_{fs} = -1.72 \text{ cm}^{-1} / \text{Fe}^{3+} \text{ ion}$

As the ferrite spinels have high order symmetry the anisotropy values are small. The anisotropy calculated for ferrous ions in magnetite is three orders of magnitude smaller than the values for ferric ions in hematite. However the antiferromagnetic resonance studies in FeF_2 show an anisotropy constant 6 to 8 times larger than that of the ferric ion in hematite. The rutile or body centered cubic magnetic structure, has each ferrous ion surrounded by a distorted octahedron of six F^- ions. The body centered sites have a symmetry rotated 90 degrees about the $[111]$ direction, producing a uniaxial symmetry. The strong crystal field quenches the orbital moment, but the second order perturbation of the spin-orbit coupling produces a large uniaxial fine structure anisotropy. Measurements on a similar material having only dipole-dipole anisotropy allows the subtraction of this contribution.

An order of magnitude calculation for the fine structure anisotropy in a $\alpha\text{-Fe}_2\text{O}_3$ crystal field gives generally good agreement also. The spin-orbit interaction on a quenched orbital electron field tends to induce a small orbital circulation dependent on the electron spin orientation. Although this will reduce the energy of the spin state,

Figure (9) Computer Program for Titanium Doped Crystals

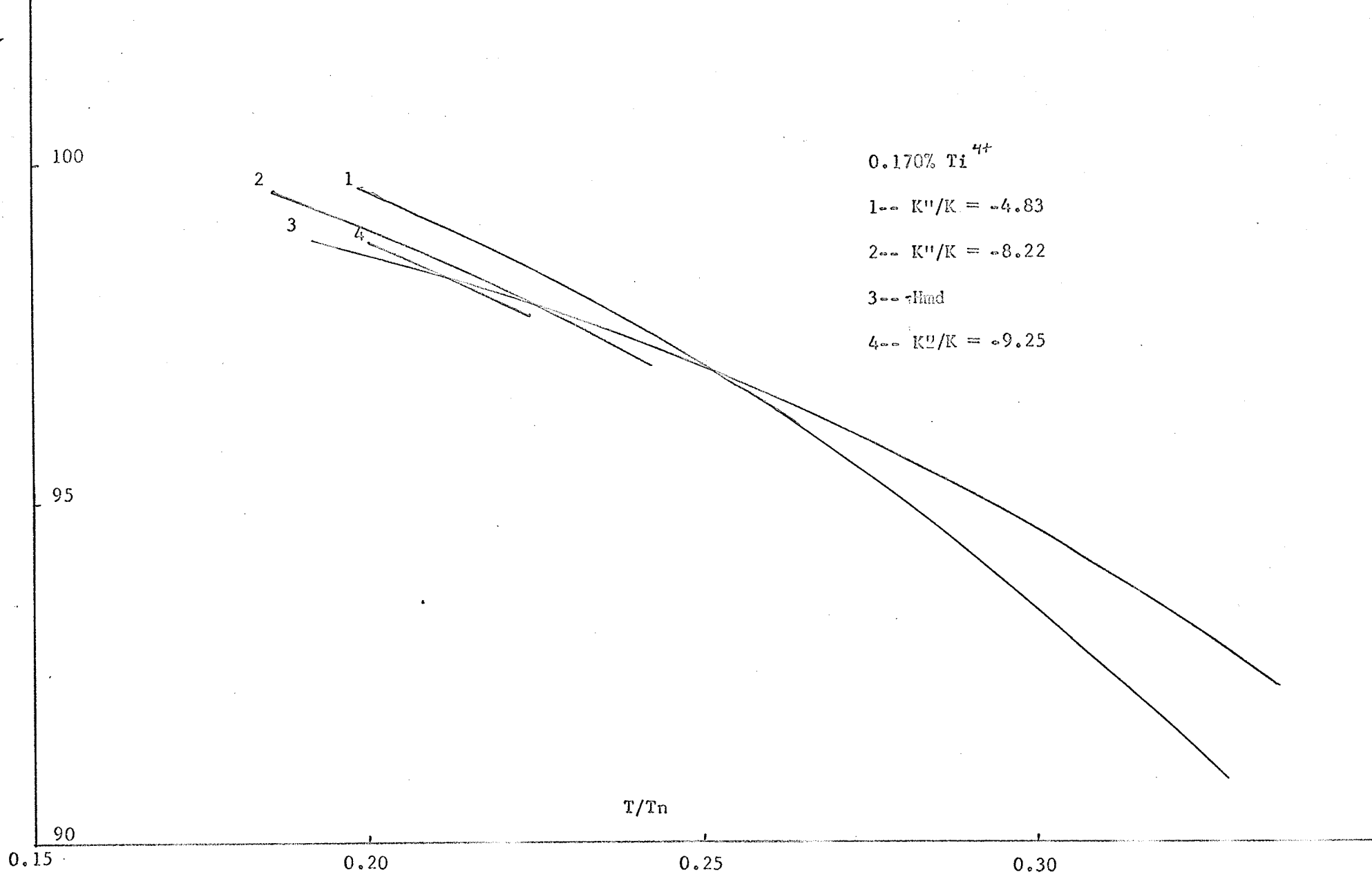
```

// EXEC FORTRAN
24 READ(1,25) DOPE,AKFS1,AKFS2
25 FORMAT(3(6X,E6.3))
   S=2.5
   WRITE(3,21) S
   XB=1.0
   TNT=.05
   BSX=1.0
1 CONTINUE
   S=2.5
   X=(3*S)*BSX/(TNT*(S.1))
   BSX=(2*S+1)/(2*S*TANH((2*S.1)*X/(2*S)))-1/(2*S*TANH(X/(2*S)))
   TEST=ABS((X-XB)/X)
   XB=X
   IF(TEST-.00001)22,1,1
22 CONTINUE
   BSX1=BSX
   BSM1=(2*(S.1)-3*BSX/TANH(X/(2*S)))/(2*S-1)*102.6
   BSM2=BSX*BSX*100.4
   BSM5=BSM2
   BSM3=BSX1
   X=X*.88889
   BSX=(2*S+1)/(2*S*TANH((2*S.1)*X/(2*S)))-1/(2*S*TANH(X/(2*S)))
   BSX1=(2*(S.1)-3*BSX/TANH(X/(2*S)))/(2*S-1)*102.6
   BSM5=.681.32*DOPE*BSX*BSX1
   BSM7=.925.82*DOPE*BSX*BSX1
   S=2.0
30 CONTINUE
   X=(3*S)*BSX/(TNT*(S.1))
   BSX=(2*S+1)/(2*S*TANH((2*S.1)*X/(2*S)))-1/(2*S*TANH(X/(2*S)))
   TEST=ABS((X-XB)/X)
   XB=X
   IF(TEST-.00001)31,30,30
31 CONTINUE
   BSM9=BSX*BSX*100.4
   BSM0=(2*(S.1)-3*BSX/TANH(X/(2*S)))/(2*S-1)*AKFS1
   BSM9=(2*(S.1)-3*BSX/TANH(X/(2*S)))/(2*S-1)*AKFS2
   BSM4=(1-11.4*DOPE)*BSM3+9*DOPE*BSM1-DOPE*BSM9
   BSM1=(1-11.4*DOPE)*BSM3+9*DOPE*BSM1-DOPE*BSM0
   BSM5=BSM7+(1-13.112*DOPE)*BSM6+.64*DOPE*BSM9
   BSM2=BSM5+(1-12.778*DOPE)*BSM6+.64*DOPE*BSM9
   X=BSM7+(1-13.112*DOPE)*BSM6
   BSM6=BSM5+(1-12.778*DOPE)*BSM6
   WRITE(3,20)TNT,BSX1,BSM8,BSM4,BSM9,BSM6
   WRITE(3,20) TNT,X,BSX,BSM1,BSM2,DOPE
20 FORMAT(1H ,2X,F3.2,5(10X,E12.6))
21 FORMAT(1H1,6HFOR S=,F4.1,40H TEMPERATURE DEPENDENCE OF ANISTROPY
11S//1H ,2X,4HTN/T,12X,8HARGUMENT,14X,8HBS(ARG.),14X,4HAKFS,18X,4H
2XKMD)
   TNT=TNT+.01
   IF(TNT-.40)1,1,23
23 CONTINUE
   GO TO 24
   END

```

Effective field oe. $\times 10^2$

Figure (9)



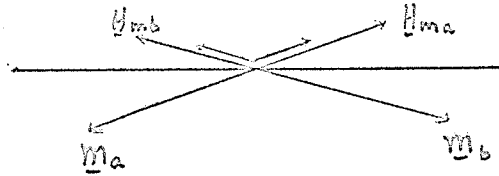
it introduces an admixture of excited orbital states into the wave function. If these orbital states lie an energy Δ above the ground state and the spin-orbit coupling is represented by λ , then the system will lie at the minimum of a Hamiltonian of the form $-x\lambda + x^2\Delta$ since the magnetic energy reduction is proportional to the amplitude of the excited state, while the electrostatic energy depends on the square of the amplitude of the excited state. The energy shift would be approximately $\lambda^2/2\Delta$ corresponding to D. Using the free ion value for $\lambda = -100 \text{ cm}^{-1}$,^{22,23} and a value Δ given by 1 to 2, $\times 10^4 \text{ cm}^{-1}$,^{9,11} this gives $|D| = \pm(0.5 \text{ to } 0.25) \text{ cm}^{-1}$, or a fine structure constant $\pm(1.5 \text{ to } 3) \text{ cm}^{-1}$ per ferrous ion. In hematite, the ferrous ion will have a smaller charge, and different crystal structure, than in the situation for the two previous values of Δ ; thus a smaller Δ (orbital splitting energy) and consequently larger fine structure would not be surprising in the actual hematite situation.

Temperature Dependence of the Ferrous Spin System

In the preceding section the temperature dependence of the ferrous ions was calculated, presuming them to be in the molecular field of one of the ferric sublattices. Since the superexchange fields are antiferromagnetic, the oppositely aligned sublattice will influence the ferrous ion exclusively to first order. The ferrous ions will lie along H_m with a temperature dependence of $B_2(x')$, where x' is the argument for spin 2 in the ferric sublattice molecular field, or $x' = 4/5 x$. The canting of the ferrous ions against the molecular field, will in general be different from the normal ferric case. If it is zero the ferrous ions will produce a small moment antiparallel to that of the ferric ions in the (111) plane (figure 10). A suitable choice of this new canting field vector \underline{D}' will give the same physical

results as the antiferromagnetic resonance three sublattice model discussed below.

Figure (10)

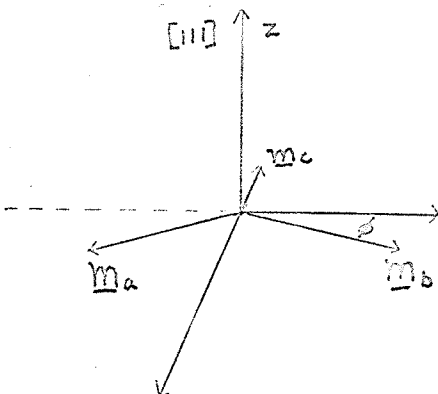


The Three Sublattice Model of Antiferromagnetism

Another model which was investigated to account for the transition shift was the three sublattice model introduced by Searle and Morrish²⁴. In this case the ferrous ions are acted on by the vector total molecular field from each sublattice $-\lambda(\underline{M}_a + \underline{M}_b)$. To a large extent these fields will cancel, leaving an x component due to the Dzialoshinski-Moriya canting. This weakly aligns the ferrous ions antiparallel to the weak ferromagnetic moment. Calculations of the free energy of the system shows additional canting energy terms are introduced by titanium substitution.

The situation above the transition temperature in the basal plane is shown in figure (11). The ferrous ions are presumed to be a third

Figure (11)



sublattice, with an interaction constant η between the third sublattice and the combined fields of the ferric sublattices.

The molecular field on the third sublattice can be written:

$$(3-3) \quad H_{mc} = -\eta(M_a + M_b)$$

As before interactions within the ferrous sublattice are zero. The

Hamiltonian of the system including Dzialoshinski-Moriya canting energy, anisotropy energy, and the interaction energy of the third sublattice

is written:

$$H = \lambda \underline{m}_a \cdot \underline{m}_b + \frac{k_1}{2} (\sin^2 \theta_A + \sin^2 \theta_B) -$$

$$3-4) - D \cdot \underline{m}_A \times \underline{m}_b + \eta (\underline{m}_a + \underline{m}_b) \cdot \underline{m}_c$$

Introducing the same coordinates and simplifications as used in

chapter I the expression becomes;

$$3-5) H = \lambda M^2 (\sin^2 \theta (\sin^2 \phi - \cos^2 \phi) - \cos^2 \theta) + 2DM^2 (-\sin^2 \theta \sin \phi \cos \phi) + k_1 \sin^2 \theta - 2\eta M M_c \cos \phi$$

for the spins lying in the basal plane at a small angle ϕ_0 , there is

a torque equilibrium when;

$$\frac{\partial H}{\partial \phi_0} = 0 = 2\lambda M^2 \sin^2 \theta \sin 2\phi_0 - 2DM^2 \cos 2\phi_0 \sin^2 \theta - 2\eta M M_c \cos \phi_0$$

or

$$3-6) 0 = 4\lambda M^2 \phi_0 - 2DM^2 (1 - 2\phi_0^2) - 2\eta M M_c (1 - \frac{\phi_0^2}{2})$$

M_c may be written as;

$$3-7) M_c = N g \mu_B S B_2(x_c) \quad S = 2.0$$

$$x_c = \frac{2g\mu_B H_c}{kT} - \frac{2g\mu_B}{kT} \hat{i} - (H - \eta (\underline{m}_a + \underline{m}_b))$$

for zero field H .

$$H_c = -2\eta M \sin \phi_0 \quad \text{to first order } \phi_0 = \frac{D}{2\lambda}$$

$$x_c = \frac{2g\mu_B}{kT} \frac{\eta}{\lambda} H_0$$

Applying experimental data from references 24 and 32, the value of

this quantity is: $\frac{\eta}{\lambda} = 2.34$ $H_0 = 2.2 \times 10^4 \text{ oe. at } T = 300^\circ \text{K,}$
and $H_0 = D \times M_a \approx B_{2.5}(x)$

$$3-8) x_c = \frac{9.2}{300}$$

Thus at room temperature the sublattice will be practically unpolarised,

with $B_2(x)$ equal to $(3)(9.2)/(6)(300) \approx 0.015$. For simplicity, the

anisotropy energy due to the increased canting is calculated for

$T = 0^\circ \text{K}$ when all sublattices are saturated. Then the magnitude of M_c

related to the sublattice magnetizations M for spins in the (111) plane

is:

$$M = \frac{N'}{2} g \mu_B S' B_S (X_A)$$

$$M_c = N g \mu_B S B_S (X_c)$$

where $N' = N^0(1-y)$ and $N = N^0 y$; y is the fraction atomic doping.

This gives:

$$\frac{M_c}{M} = \frac{y}{1-y} \frac{4}{5} = R = \frac{4}{5} y (1+y+y^2) \quad (T=0^\circ K)$$

Returning to solve (3-6) the result is:

$$\phi_0^2 (\eta r + 4D) + \phi_0 (4\lambda) + (-2D - 2\eta R) = 0$$

To first order for small ϕ_0 :

$$\phi_0 = \frac{D + \eta R}{2\lambda}$$

The anisotropy energy between the two orientations will be the

energy at $\theta = 90$ degrees minus the energy at $\theta = 0$. Substituting (3-10)

in (3-5) and evaluating the difference gives:

$$\begin{aligned} \Delta E &= \lambda M^2 - \lambda M^2 \cos 2\phi_0 - D M^2 \sin 2\phi_0 + k_1 - 2\eta M^2 R \sin \phi_0 \\ &= \lambda M^2 - \lambda M^2 \left(1 - \frac{4}{2} \left(\frac{D + \eta R}{2\lambda}\right)^2\right) - D M^2 \left(\frac{D + \eta R}{\lambda}\right) + k_1 - \frac{2\eta M^2 R}{2} \left(\frac{D + \eta R}{\lambda}\right) \end{aligned}$$

and ΔE becomes:

$$\begin{aligned} \Delta E &= k_1 + M^2 \left(\frac{D + \eta R}{\lambda}\right) \left[\lambda \frac{(D + \eta R)}{2\lambda} - D - \eta R\right] \\ &= k_1 - M^2 \left(\frac{D + \eta R}{\lambda}\right) \left(\frac{D + \eta R}{2}\right) \\ &= k_1 - \frac{H_0^2}{2\lambda} - \frac{\eta}{\lambda} H_0 M R - \frac{\eta R^2}{2\lambda} M^2 \\ &= k_1 - \frac{H_0^2}{2\lambda} - \frac{\eta}{\lambda} H_0 M R - \left(\frac{\eta}{\lambda}\right)^2 \frac{R^2}{2} H_m M \end{aligned}$$

The magnitudes of these terms are estimated using:

$$\lambda = \frac{1}{\chi_1} = \frac{1}{1.93} \times 10^5 = .518 \times 10^5 \quad \frac{\eta}{\lambda} = 2.34$$

$$H_0 = .22 \times 10^5 \quad y = 2.6 \times 10^{-3} \quad M = 920 \text{ emu/cc} \quad H_m = 9 \times 10^6 \text{ oe.}$$

and expressing ΔE as an effective field:

$$\frac{\Delta E}{M} = \frac{k_1}{M} - 27.2 - 106.8 - 166 \text{ oe}$$

but near room temperature the field will become:

$$\begin{aligned} \frac{\Delta E}{m} &= \frac{k_1}{m} - 27.2 - 107 (.015) - 166 (.015^2) \\ 3-12) \quad &= \frac{k_1}{m} - 27.2 - 1.6 = \frac{k_1'}{m} - 1.6 \text{ oe} \end{aligned}$$

Figure (12) shows transition temperature prediction curves using this method. Since the third sublattice is weakly aligned and gives essentially no contribution to K_1 . The ferrous ions contribute no anisotropy energy to either K_{nd} or K_{fs} . The curves for the remaining anisotropy energies intersect at $T_m = 280$ K. The field of 2 oe. shifts this value negligibly. However if these additional negative energy terms are large enough to exceed the difference between H_{nd} and H_{fs} from the crossover point to $T/T_m = 0$ then the spins are always in the basal plane, and the transition is suppressed. Figure (12) contains curves for a doping of 0.26% Titanium. Experimentally the transition is suppressed in this material. The energy difference between the curves at $T = 0$ K is 261 oe. Thus, although the values of ΔE for an almost saturated third sublattice, even at room temperatures, would be sufficient to suppress the transition completely, it is obvious that the model of a weakly aligned third sublattice, while successful in interpreting resonance data, gives a completely wrong transition temperature shift. Even if this theory was retained, to the exclusion of all else, and the actual opposite shift blamed on another type of ferrus single ion anisotropy, the magnitude of this $D(0)$ necessary can be calculated by evaluating equation (2-15) in the paramagnetic region together with the results of (3-1), (3-8), and table IV.

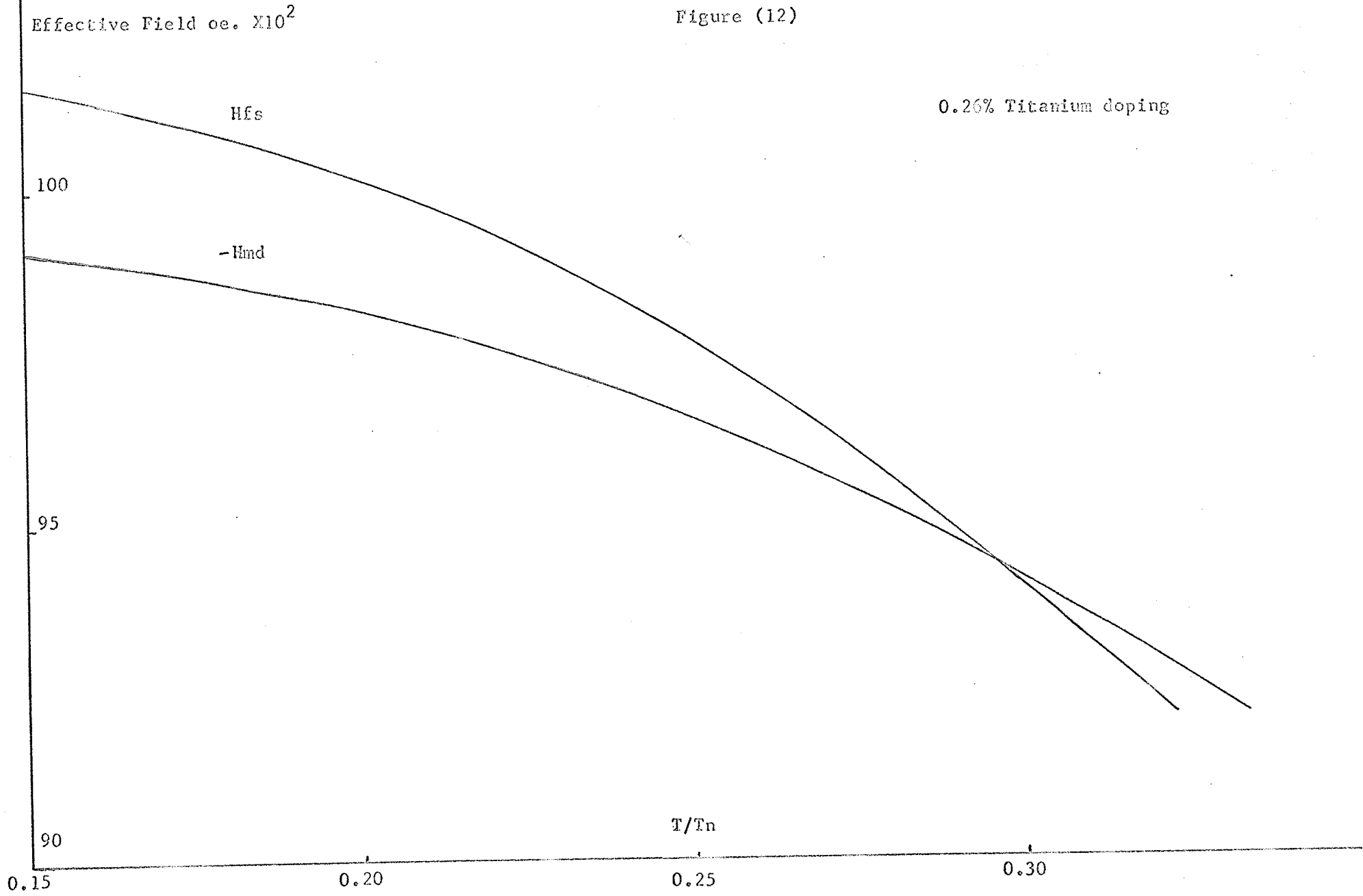
$$D(0) \left(\frac{S+1}{3S} - \frac{3}{2S} B_S(x_c) \coth \frac{x_c}{2S} \right) = 8.22 (1.2) \text{ cm}^{-1}$$

simplifying the expression for small argument x :

$$D(0) \left(\frac{3}{2} - \frac{3}{4} \left(\frac{S+1}{3S} x_c \right) \left(\frac{2S}{x_c} + \frac{x_c}{6S} \right) \right) = 8.22 (1.2)$$

$$D(0) \left(\frac{-x_c^2}{16} \right) = 8.2 (1.2)$$

Figure (12)



$$3-13) \quad D(0) = \frac{-16(8.22)(1.2)}{\left(\frac{9.2}{300}\right)^2} \approx -1.6 \times 10^5 \text{ cm}^{-1}$$

There is no possible mechanism by which such a large anisotropy can exist, the largest value occurring naturally being $< 10^2 \text{ cm}^{-1}$ ^{29,16}; thus the weak third sublattice theory is untenable for this data.

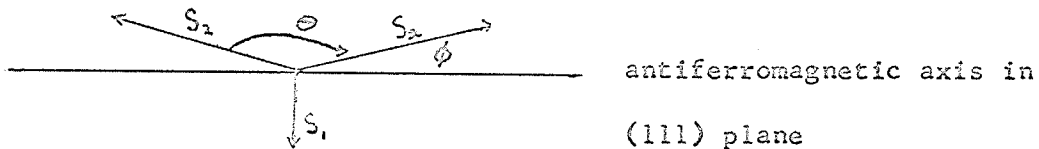
Self-Trapping and Double Exchange.

A model which could reconcile the difficulty of the weak third sublattice at room temperature was suggested by the articles of Anderson²⁶ and De Gennes²⁷ on "double exchange". The addition of small dopings of titanium in hematite increases the conductivity by many orders of magnitude, supporting the picture of hopping electrons transferring between ions of opposite spin. The indirect spin coupling interaction arising from this mobile electron exchange is a function of the spin orientation of both ions participating in the transfer. By suitable approximations the energy interaction term can be written²⁷

$$E = \frac{1}{2} b S_1 S_2 \cos \frac{\theta}{2}$$

corresponding to the three spin terms arranged as in figure (13)

Figure (13)

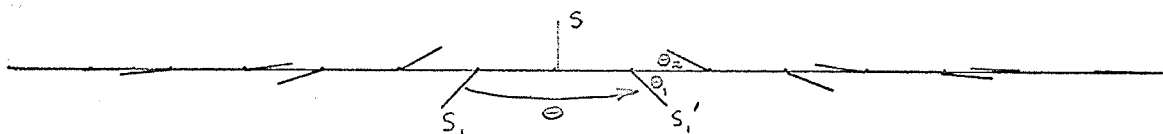


where the S_2 's belong to each iron atom of the nearest neighbour pair.

In layer antiferromagnets, such as $\alpha\text{-Fe}_2\text{O}_3$, it is sometimes preferential for a carrier to build up a local spin distortion in the lattice by which it is self trapped,^{27,40} and subsequently can only move

slowly through the lattice. If such a situation can occur in hematite it can be thought of as a pair of ferric ions sharing the same mobile electron. The large time spent on one ion (10⁻¹⁰ seconds) plus effective mass data^{38,39} indicate agreement between this model and experimental evidence. The mobile exchange electron lies in torque equilibrium in the basal plane, under the actions of the super-exchange field, the double exchange transfer integral effective field, and the canting field. Also the increased cantings of the ion pair warps spins from the antiferromagnetic axis for all the nearest neighbours forming a spin warp tail much like a domain wall in energy density. Figure (14) is a diagram of a simple 1 dimensional model of the possible spin warp tail.

Figure (14)



The Hamiltonian of this system can be written:

$$\begin{aligned}
 \mathcal{H} &= 2b \cos(\theta_i + \frac{\pi}{2}) S S_1 + 2J \cos(\pi - 2\theta_i) S_1^2 \\
 &+ \sum_i \left[2J \cos(\pi - (\theta_{i+1} - \theta_i)) + D S_1^2 \sin(\pi - (\theta_i - \theta_{i+1})) \right] \\
 &+ D \sin(\pi - 2\theta_i) \quad \text{where} \quad S = \frac{1}{2} \quad \text{and} \quad S_1 = \frac{\sqrt{5}}{2}
 \end{aligned}$$

In all the following, the spins are classical vectors with small angle differences in the tail region. From the above Hamiltonian, neglecting tail energy and canting energy the equilibrium condition

is:
$$\sin \theta_i = \frac{b}{2J} \frac{S}{S_1}$$

The magnetic moment of the system (S_1 , S_1' , and S) will be:

$$-14) \quad M = \mu_B (2S_1 \sin \theta_1 - S)$$

Experimentally, there is no measurable increase in the magnetic moment of the titanium doped samples, thus it is required that $M = 0$ or $\sin \theta = S/2S_1 = 1/10$, corresponding to $\theta = 6$ degrees and $J = b$.

$$-15) \quad \text{The exchange energy of the canted spin tail can be calculated as: } E = -2JS_1^2 \sum \cos \Delta \theta_{ij} \quad \text{when } \sum \Delta \theta_{ij} = \theta_1$$

For a small linear change in spin orientation over n sites the approximation holds that $\cos \theta = 1 - \theta^2/2$, and $\Delta \theta = \theta_1/n$:

$$-16) \quad E = -2JS_1^2 n + JS_1^2 \sum (\Delta \theta_{ij})^2 \\ = -2JS_1^2 n + \frac{JS_1^2 \theta_1^2}{n}$$

corresponding to:

$$-17) \quad E_{\text{Ti}} = \frac{JS_1^2}{n} \sin^2 \theta$$

Expression (3-16) does not have a finite minimum, indicating that for vanishingly small dopings the mobile electrons would shift the direction of the sublattice in the basal plane, unless there exists impurity or defect pinning of either. For our dopings, in addition to any other effects, the spin-warp tails will overlap in increasing numbers as the tails grow larger. Investigating diagrammatically, either ferromagnetic or antiferromagnetic arrangements of ion pairs will have a minimum energy. Thus it is likely that the third sublattice will still be weakly polarised in the (111) plane.

But for spins canting out of the (111) plane, the restoring torque will be from the exchange energy of the tails (equation 3-17); which is the normal molecular field divided by n , the number of ions in the tail. For our dopings, the average number of ions between mobile

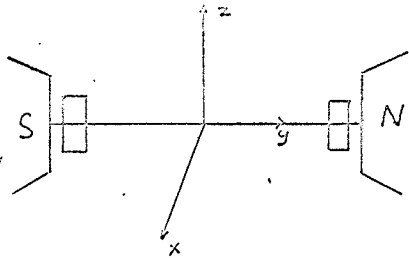
electrons is never greater than ten. In addition to this energy, the normal molecular fields act on the two ferric ions; and through the transfer integral b , on the mobile electron. Thus for orientations into the z direction, the ferrous ions will be more strongly bound to the basal plane than in the case of model I; and in both these models the third sublattice will be almost saturated in the basal plane for temperatures above the transition, and thus contribute to a part of the dipolar and fine structure energy. Only in this way can the three sublattice model be applicable to these computations.

Chapter IV

Description of the Equipment and Technique

Measurements of the magnetization of doped single crystal hematite were taken using a Vibrating Sample Magnetometer manufactured by Princeton Applied Research. A constant homogeneous magnetic field of up to 19 koe. was supplied by a Magnion 12 inch electromagnet and constant current supply.

The Vibrating Sample Magnetometer was invented by S. Foner⁴¹. A magnetic sample, smaller than a $\frac{1}{2}$ inch cube, is fastened to a vibrating sample holder which moves sinusoidally along the z direction. The movement of this magnetic dipole induces a current in two pickup coils attached to the magnet pole faces.



This current will be proportional to the magnetization of the sample, if the sample can be treated accurately as an equivalent point magnetic dipole. The current from the pickup coils is amplified and averaged in the instrument, and then compared with a reference signal determined by the motion of the sample holder. This measurement procedure gives a reading proportional to the magnetization of the sample, but insensitive to the amplitude of vibration or the stability of that amplitude. However the reading depends strongly on the position of the sample between the pickup coils. To remove this difficulty, before taking any reading the position of the sample is adjusted to the geometrical center of symmetry of the pickup coil arrangement. This position can be found repeatedly by moving the sample along the three axes so that the magnetization reading is at a minimum for movements along the y axis, and a maximum for movements along the x or z axes.

Therefore if all samples are adjusted to the geometrical center before taking a measurement the geometrical effects will be constant.

Magnetization readings for samples at this point can then be compared with equivalent readings from materials whose magnetization is known to obtain an absolute calibration of the magnetic moment. While the instrument is sensitive to changes of 5×10^{-5} emu. in the magnetization of the sample, system noise and vibration makes it impossible to adjust the sample position repeatedly to the accurate geometrical center when the sample moment is very small. The technique evolved for measurements on hematite, calibrated all moments relative to the moment of a bar of spectroscopically pure nickel. Since the electronic balancing and amplification system of the instrument drifted appreciably over a few days; before each period of measurement the nickel sample was mounted and adjusted to the geometrical center or "saddlepoint" position. The magnetization curve of the nickel sample was then taken and graphically analysed to give a reading of the saturation magnetization and susceptibility. These readings were proportional to the actual values for a pure nickel sample of equal weight, as determined from C.R.C. tables or other references. This constant of proportionality was then evaluated, and any following reading could be multiplied by it, to yield directly the magnetic dipole moment in emu. per gram; providing it was accurately positioned at the geometrical center. Due to the electronic drift the calibration was repeated daily or whenever other adjustments on the machine were changed.

Using this method, various samples were mounted, and magnetization

curves taken at room temperature. Differences between dopings were in general quite small, only a few times larger than the system error. When two to four measurements were taken for each sample, agreement was generally within one percent, except for those with very small weak signals. Between each measurement the sample was removed, inspected, and if necessary remounted on the sample holder. It was then replaced in the instrument and readjusted in orientation and geometrical position. Due to these precautions there should be no systematic error in these results.

The low temperature measurements were made with an Andonian liquid helium metal dewar using liquid nitrogen for coolant in a variable temperature sample cavity. The dewar was specially designed for compatibility with the P. A. R. magnetometer; having a long vacuum insulated stainless steel tail extending between the signal pickup coils and supported from the magnetometer assembly. It thus takes the place of the normal outer tubular casing which constrains the vibration of the sample holder along the z axis. The sample chamber itself is arranged in the dewar tail so that it is above an electrical heater surrounding the outlet of a capillary tube and expansion valve, through which coolant can flow from an insulated reservoir.

In practice the throttle valve is opened to a reasonable liquid nitrogen flow rate. The nitrogen escapes from the outlet of the capillary tube and evaporates to nitrogen gas at a temperature of 77 degrees Kelvin. As it rises up the sample chamber it can be heated to any temperature necessary by varying the electrical current in the

heater winding. The temperature of the sample is thus controlled by that of the gas. With this system it was not possible to attain a true equilibrium temperature and stay at that constant temperature for a great enough time to get an entire magnetization curve. Using a battery and rheostat to give a constant current supply to the heater winding, the temperature still varied slowly: a degree every few minutes. In the critical transition region this would be unacceptable and the best stability was obtained only near room temperature in any case. The temperature runs were made cooling the sample slowly to liquid nitrogen temperature. By regulation of the liquid nitrogen flow-rate and heater current the temperature of the sample fell about 5°K per minute, or less if in the transition region.

The temperature of the sample was measured by a Copper-Constantan thermocouple directly in contact with it, and the vibrating sample holder. In order to minimise the thermal lag, the thermocouple was constructed of number 30 wire with a thin flat join, glued in contact between the sample and the holder. The potential of the thermocouple in series with an ice bath cold junction was indicated on a digital millivoltmeter. Readings were converted to the Centigrade or Kelvin temperature scales to within the nearest half degree.

With this technique measurements could be made from $+40^{\circ}\text{C}$. to -150°C . At the lower end of the temperature scale the sample temperature control functioned poorly, usually dropping the last 20 to 30 degrees in a few seconds. In addition at low temperatures below the transition, the moment signal was only slightly larger than background noise. At these temperatures, strange fluctuations occurred which probably were of instrumental origin. In most cases such effects

were small and could be neglected, or corrected for as part of the background signal measured without a sample. In cases of weak signal this background was subtracted in the analysis to leave an accurate magnetization measurement. The raw data consisted of curves of magnetization versus temperature for several constant field points. For certain values of temperature the magnetization curves of M versus H were drawn. Extrapolation of the linear portion of the curve yielded values of χ and M_0 , the susceptibility and spontaneous moment in the direction of the magnetic field respectively. These values at $T = 20^\circ\text{C}$. gave calibrations from the room temperature data taken earlier. No attempt was made to calibrate directly to the nickel sample since the magnetization signal of a sample in the dewar was halved due to the shielding effect of the metal walls; and therefore the geometrical adjustments were too difficult with the dewar in position.

By the alignment of the crystal on the sample mount, and the provision of an azimuthal orientation control on the magnetometer, measurements could be made in two crystallographic directions: along the $[111]$ direction, and along a certain direction in the basal plane. With the accuracy of the original X-ray crystallographic orientation being better than one degree, these directions would also be correct to within a degree.

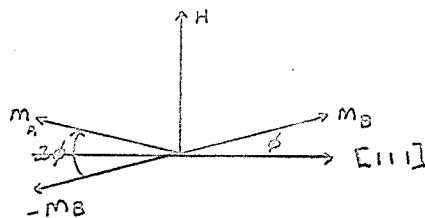
Interpretation of Results

The experimental results will be interpreted in two sections, firstly the temperature ranges outside the transition region, and secondly the transition region itself.

Below the transition region the hematite crystal behaves as a normal antiferromagnet, whose behaviour may be described adequately by a classical two sublattice molecular field calculation. Although the orientation of the sublattices is fixed by the anisotropy terms, these effective fields are negligible, in comparison to the isotropic superexchange fields. The applied field H , cants the sublattices from the antiferromagnetic axis against the torque of the superexchange field. The small (217 oe. or much less) anisotropy fields have negligible effect in comparison to the two large fields, and therefore are discarded from all ensuing calculations. In the experiment fields were applied parallel and perpendicular to the $[111]$ direction.

χ_{\parallel} and χ_{\perp} are defined as the susceptibilities parallel and perpendicular to the antiferromagnetic axis. Solving for the susceptibilities^{8,29} below the transition temperature it is necessary to write down only torque equilibrium conditions for the system of figure (15). The magnetic sublattices are canted off the z axis through an angle ϕ by the applied field H . It is required that H be much less than the field which will flip the spins onto the basal plane (treated in a following section). Then the total torque on M_a must be zero:

Figure (15)



$$4-1) \quad |M_A \times (H + H_{m_A})| = 0$$

$$|M_A \times H - \lambda M_A \times M_B| = 0$$

Simplifying the expression;

$$4-2) \quad M H \cos \phi - \lambda M^2 \sin 2\phi = 0$$

$$\text{and} \quad 2M \sin \phi = \frac{H}{\lambda}$$

however the moment produced by the canting is also $2M \sin \phi$, thus representing the moment measured by the magnetometer (m). Thus;

$$4-3) \quad m = \frac{H}{\lambda} = \chi_{\perp} H$$

and the perpendicular susceptibility is;

$$4-4) \quad \chi_{\perp} = \frac{1}{\lambda}$$

the inverse of the molecular field constant, and thus constant with temperature, if λ is constant with temperature.

The situation for χ_{\parallel} , the susceptibility in the $[111]$ direction antiferromagnetic axis is more complicated as the degree of saturation of the magnetic sublattices is important. Theoretically, at saturation χ_{\parallel} will be zero since H will exert no torque on the oppositely aligned sublattices.²⁹ However, for non zero temperatures H exerts a torque on the nonaligned spins and polarises a small moment in the z direction. Since the nearest neighbour direct exchange constant has been presumed zero in all previous hematite calculations, for reasons discussed in chapter I, the results of Lidiard²⁸ as shown in a text by Morrish²⁹ can be applied to this situation. Lidiard shows a curve for the predicted temperature dependence of $\chi_{\parallel} / \chi_{\perp}$ below the Néel temperature, when the interaction constant between ions of the same sublattice can be neglected. Only the lower portion of the curve, below the transition region will be measurable, and in this region the values of χ_{\parallel} are expected to be extremely small.

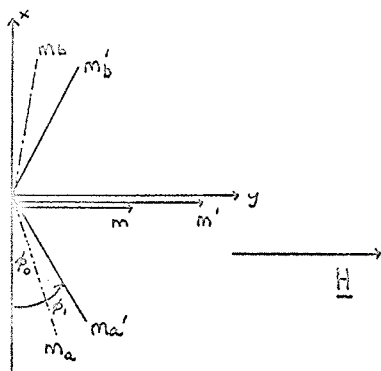
For the experiments where system noise did not swamp the measurements of these small signals, the theoretical curves are plotted as a comparison.

The behaviour below the transition region is therefore expected to be linear, with zero spontaneous moment for directions both parallel and perpendicular to the $[111]$ direction.

Above the transition, with spins in the (111) plane, the weak magnetic moment due to the canted sublattices appears. With the field applied in the $[111]$ direction, it exerts a torque which cants the spins out of the (111) plane against the molecular field. The moment measured in the $[111]$ direction is due exclusively to this canting, and by arguments identical to those developed previously, it is clear that the magnetization curves will be linear with zero spontaneous moment, and perpendicular susceptibility $=1/\lambda$.

When the field H is applied in the basal plane, the interaction energy between the field and the weak moment is at a minimum when the weak moment is lined up in the direction of the applied field. Since the anisotropy fields in the basal plane are on the order of one oersted¹¹, this lining up process, or saturation of the weak moment, should occur at very low applied fields. At a sufficiently high field, H will then be perpendicular to the canted sublattices (figure (16)), and again the magnetization will vary linearly with field as the

Figure (16)



spins are canted against the molecular field - M . The magnetization curves will rise swiftly to a saturation value, and then become linear with

susceptibility:

$$(4-5) \quad \chi_{\perp} (111) = \frac{1}{\lambda}$$

In aluminum and gallium substitutions, the nonmagnetic ions should not alter this picture greatly, except for a change in the transition temperature region. Although a slight decrease in moment might be expected, a decrease in molecular field could make up for this.

In the two physical models for the titanium substitution that were considered, the ferrous sublattice is either only slightly polarised or its component ions are divided equally between the antiferromagnetic A and B sublattices. In such a case one would again expect to see only a very slight effect with the addition of titanium doping.

The spontaneous weak moment, as discussed earlier, is derived from the Dzialoshinski-Moriya interaction canting of the sublattices in the basal plane. Thus it is proportional to the degree of saturation of the magnetic sublattices. It will have the temperature dependence of the normal Brillouin function with Néel temperature 948°K . In the small range of temperature above the transition region measurable with this equipment, this takes the form of a barely discernable decrease in saturation moment with increase in temperature.

In the transition region, the increased width of the transition is thought to be a function of inhomogeneous doping. A sharp transition would occur in a microscopic volume of constant doping, when the temperature fell below that for the predicted transition. To confirm this hypothesis, the electron microprobe analysis results of Besser et al.,¹¹ were used to estimate the inhomogeneity of doping in the experimental samples. These measurements were taken a few mm. along the smooth faces of single crystals doped with Ca^{2+} or Ti^{4+} . The doping of the Ti^{4+} sample varied continuously over a concentration of $0.0017 \pm 42\%$. On the gallium sample, 10% of the

trace was discontinuous at 300% \pm 50% of the normal concentration. These discontinuities were interpreted visually as etch pits in the crystal surface, or inclusions of a separate phase of the crystal, perhaps Ca_2O_3 . In order to test the theory that these inhomogeneities broaden the theoretically sharp transition, the variation in doping throughout the specimens was presumed to follow a Gaussian distribution of the volume. The standard deviation of the distribution was considered approximately the same as the limits given previously for the microprobe analysis. The results of chapter II and III were then used to predict the transition temperatures for dopings of points on this Gaussian curve. At any doping point corresponding to a transition temperature prediction T_m^1 , the area of the curve of greater dopings with lower transition temperatures would contribute moment m_0 , while the rest of the curve will have completed the transition and contribute moment zero. Thus theoretical transition curves were prepared, and can be compared with experimental results.

Another possible method of transition broadening is with a non-zero value of the second order anisotropy constant. Reference 11 reports conflicting evidence on this subject. While K_2 is usually taken as zero, neutron diffraction experiments report a 5 degree canting off the $[111]$ direction at 4°K. Writing the anisotropy energy to second order;

$$(4-6) \quad E = k_1 \sin^2 \theta + k_2 \sin \theta$$

there is equilibrium for; $\frac{\partial E}{\partial \theta} = 0$
 $2k_1 \sin \theta \cos \theta + k_2 \sin^2 \theta \cos \theta = 0$
 $k_1 \sin 2\theta + 2k_2 \sin^2 \theta \sin 2\theta = 0$
 giving a value of $\theta = 0$ or $\theta = 90$ or:

$$(4-7) \quad \sin^2 \theta = \frac{-k_1}{2k_2}$$

This would imply that K_2 is large and negative. Indeed, to fit the neutron diffraction data $K_2 = -2K_1 \times 10^4$, a surprising figure. Any broadening of the transition from this source would have to occur through the third minimum (4-7) where $0 < \frac{-K_1}{2K_2} < 1$. If K_2 is not zero, at this point, and can be treated as a constant over a limited temperature range, the width of the transition should be related to the difference between H_{md} and H_{fs} at a temperature one half transition width away from the crossover point; through the square of the sine of this difference. Any linearity in a plot of these quantities could possibly imply such a happening, provided the original hypothesis is discarded.

Another topic of interest in the data is the field induced transition which can be caused by a strong field applied either along the $[111]$ direction, or in the basal plane.

A field in the $[111]$ direction induces the spin flop process. An explanation of this is given in reference (11). For reasonable approximations the required field is:

(4-8)

$$H_{sf} = \sqrt{2H_m H_a} \quad H_a = K_1 / M$$

When a strong field is applied in the (111) plane, additional canting of the sublattices increases the second energy term in equation (3-12). This additional canting energy can be calculated by including the applied field H in the x direction, in the free energy expression (1-14). Then solving for equilibrium at $\theta = 90$ degrees;

(4-9)

$$H = \lambda M^2 (-\cos 2\phi) - D M^2 \sin \phi - 2 H M \sin \phi$$

for equilibrium $\phi_0 = \frac{H_d + 2H}{2H_m}$, the anisotropy energy becomes:

(4-10)

$$\frac{\Delta E}{M} = \left[\frac{(H_0^2 + 2H_0 H_m)}{2H_m} \right] \text{ or } \Delta E = - \left[\frac{H_0^2}{2\lambda} + \frac{H H_0}{\lambda} \right]$$

Increase in this term of the anisotropy energy makes the (111) plane more preferable to the sublattices, and the transition will reverse if $H H_d/H_m$ is greater than the difference between the two curves at a given temperature, as plotted from the results of chapters IX and III. As the polar dependence of this term is unknown the field induced transitions may not be sharp. Models of the same effect have been proposed by references 30 and 31, but our data does not agree with their predictions.

Having discussed the methods for calculating curves of spontaneous moment versus temperature, and transition temperature versus applied field; a combination of both these methods is used to predict the behaviour of the susceptibility with temperature. The same postulates are used as previously. The doping throughout the crystal is given by a Gaussian distribution of the volume. For a small volume of constant doping, the transition, even if field induced, is sharp when the temperature falls below the predicted transition temperature. Below the transition the material has zero spontaneous moment, and susceptibility $\chi_{\perp} = 1/\lambda$, as shown earlier.

Firstly for a field applied in the (111) plane, the magnetization will be;

$$4-11) \quad m = (m_0 + \chi_{\perp} H) R + (1 - R) \chi_{\perp} H$$

where, R is the fraction of material which has not undergone the transition at temperature T, and χ_{\perp} is the constant value $1/\lambda$.

Differentiating this gives for χ ;

$$4-12) \quad \chi_{\perp}(T) = \chi_{\perp} + m_0 \left(\frac{\partial R}{\partial H} \right) + R \frac{\partial m_0}{\partial H} = \frac{\partial m}{\partial H}$$

and the terms may be evaluated by expanding the formula as:

$$4-13) \quad \chi_{\perp}(T) = \chi_{\perp} + m_0 \left(\frac{\partial R}{\partial \left(\frac{T_m}{T_N} \right)} \right) \left(\frac{\partial \left(\frac{T_m}{T_N} \right)}{\partial \Delta E} \right) \left(\frac{\partial \Delta E}{\partial H} \right)$$

The second term has been split into three factors, each of which can be evaluated from the computer graphs.

$\left(\frac{\partial R}{\partial T}\right)$ -- This term is the derivative of the fraction of material which has not undergone the transition, with change in temperature, providing there is a Gaussian distribution of μ parts, as in the spontaneous moment calculation. This factor will be proportional to the slope of the spontaneous moment versus temperature curve.

$\left(\frac{\partial \left(\frac{T_M}{T_N}\right)}{\partial \Delta E}\right)$ -- This term is the change in transition or crossover point, for a small addition of energy ΔE to the positive fine structure energy. It is calculated as the slope of Hf_s minus the slope of $-Hm_d$.

$\left(\frac{\partial \Delta E}{\partial H}\right)$ -- This will be the derivative of the change in anisotropy energy due to increased canting; with respect to the applied field H .

In the case of H lying in the basal plane, this becomes the derivative of the term Hm_d/Hm , or Hd/Hm a constant with respect to applied field.

All three of these terms were evaluated from table V, the spontaneous moment curves, and the anisotropy energy curves, and are to be compared with the experimental susceptibilities in the (111) plane.

In the [111] direction the process is similar, and since $\chi_{||} \approx 0$ thus:

$$4-14) \quad \chi_{||}(\tau) = \chi_{\perp} H R + \chi_{||} (1-R) = \chi_{\perp} \left(R + H \frac{\partial R}{\partial H} \right)$$

$\frac{\partial R}{\partial H}$ is evaluated by the same method used previously, except now $\frac{\partial \Delta E}{\partial H}$ is the derivative of the spin flop field $H^2/2Hm$, and thus equals H/Hm .

The susceptibility becomes:

$$4-15) \quad \chi_{||}(\tau) = \chi_{\perp} \left[R + H^2 \left(\frac{\partial R}{\partial T} \right) \left(\frac{\partial \left(\frac{T_M}{T_N}\right)}{\partial \Delta E} \right) \frac{1}{Hm} \right]$$

For the [111] direction, the susceptibility should be parabolic in H at lower temperatures, all other factors remaining constant, while in the (111) plane the susceptibility is constant, and the magnetization curve should remain linear even in the transition region, if the other derivatives are constant with respect to H (true only in small regions).

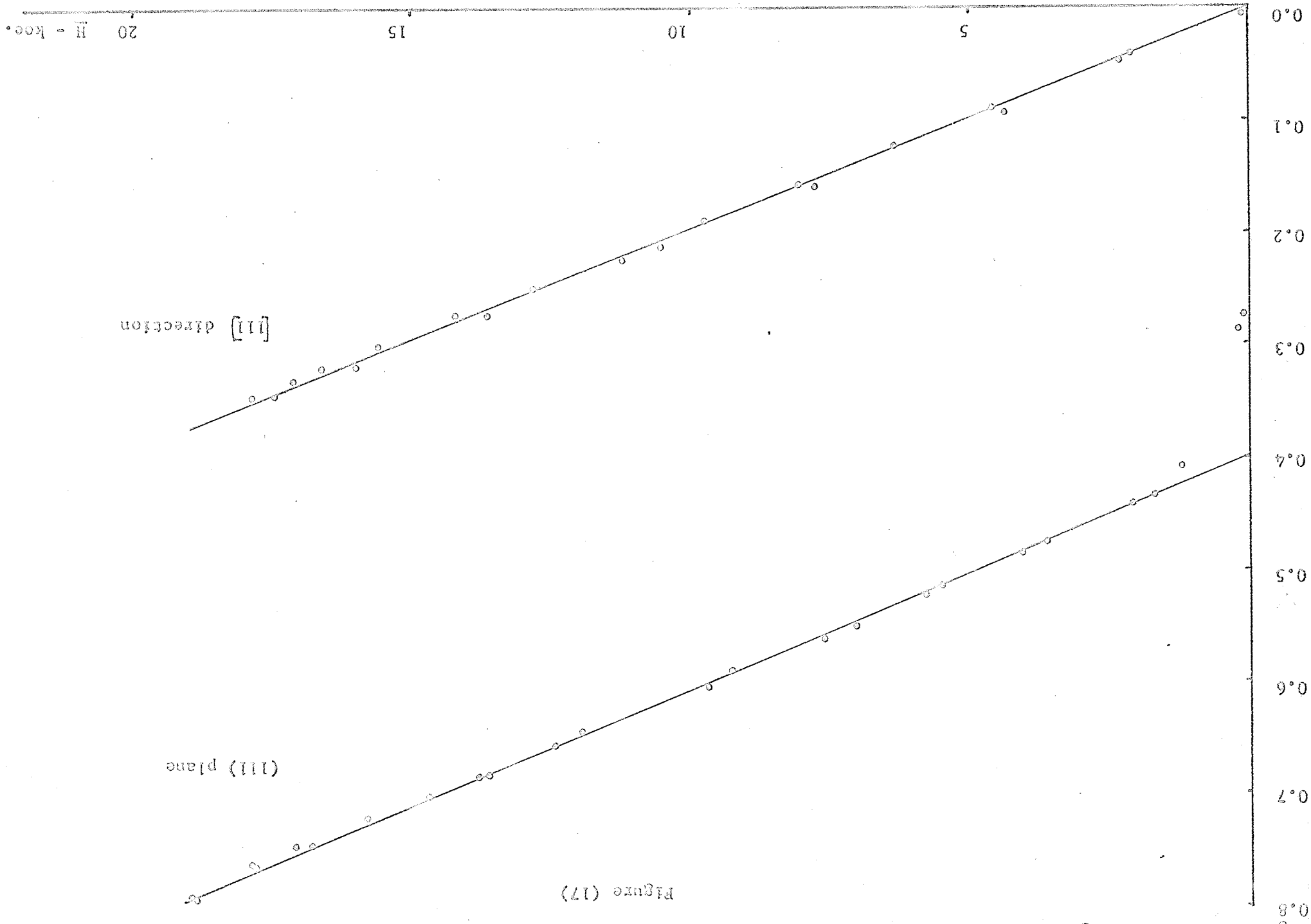


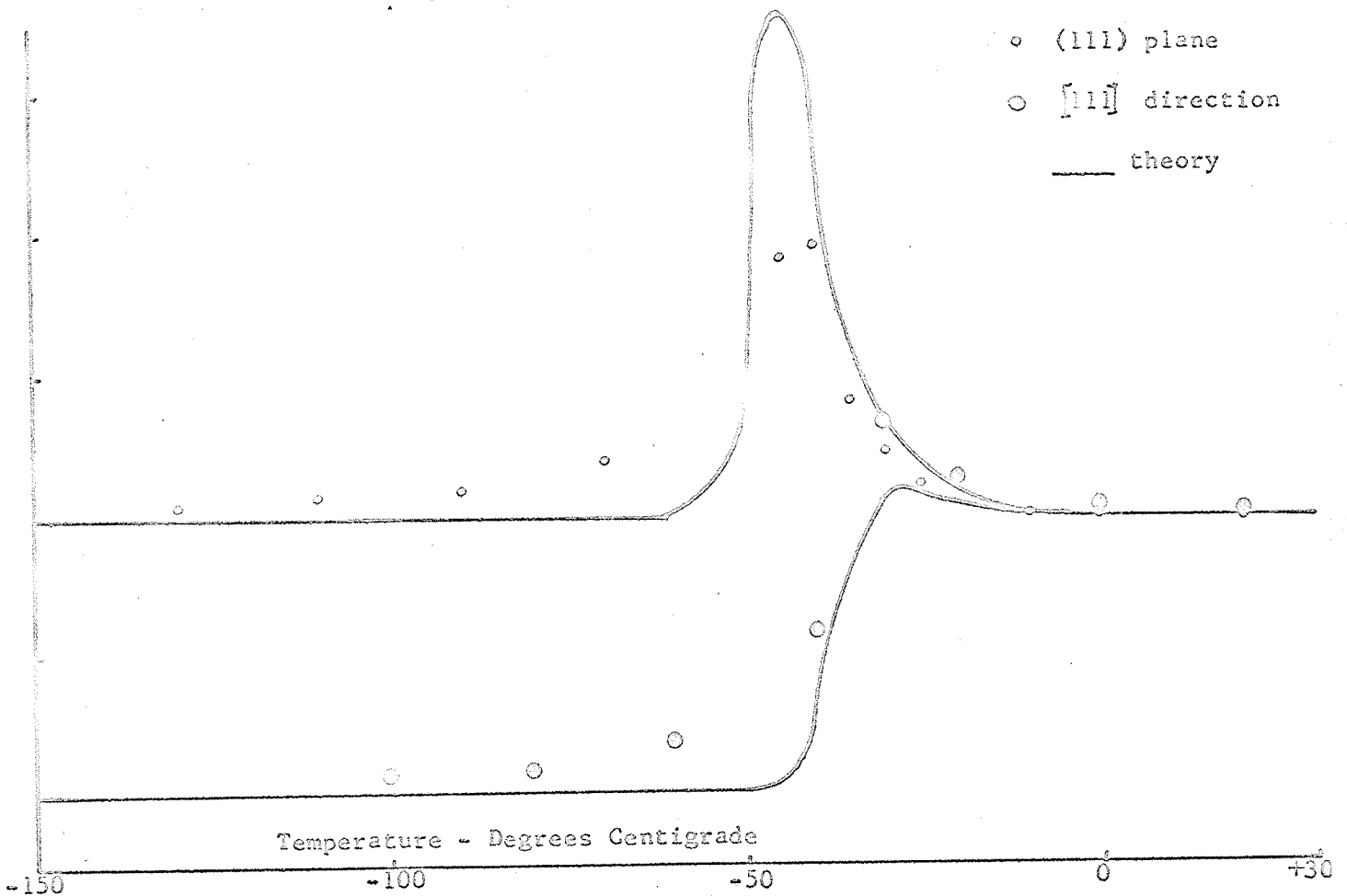
Table V

Room Temperature Data

Doping	χ [111] = $1/\lambda$	χ (111) = $1/\lambda$	M_0 emu./gm.	H_d = $2\lambda M_0$ koe.	H_m = λM oe. $\times 10^6$
atomic %	emu. per gm.-oe. $\times 10^{-6}$		emu./gm.	koe.	oe. $\times 10^6$
pure	19.35	19.3	0.412	21.3	9.12
2.06% Al	19.8	19.6	0.420	21.4	8.98
1.38% Ga	20.4	19.6	0.417	21.2	8.63
0.170% Ti	19.1	19.3	0.422	21.6	8.89
0.258% Ti	19.9	19.9	0.428	21.5	8.84
0.353% Ti	----	20.2	0.431	21.3	8.71

Figure (18)

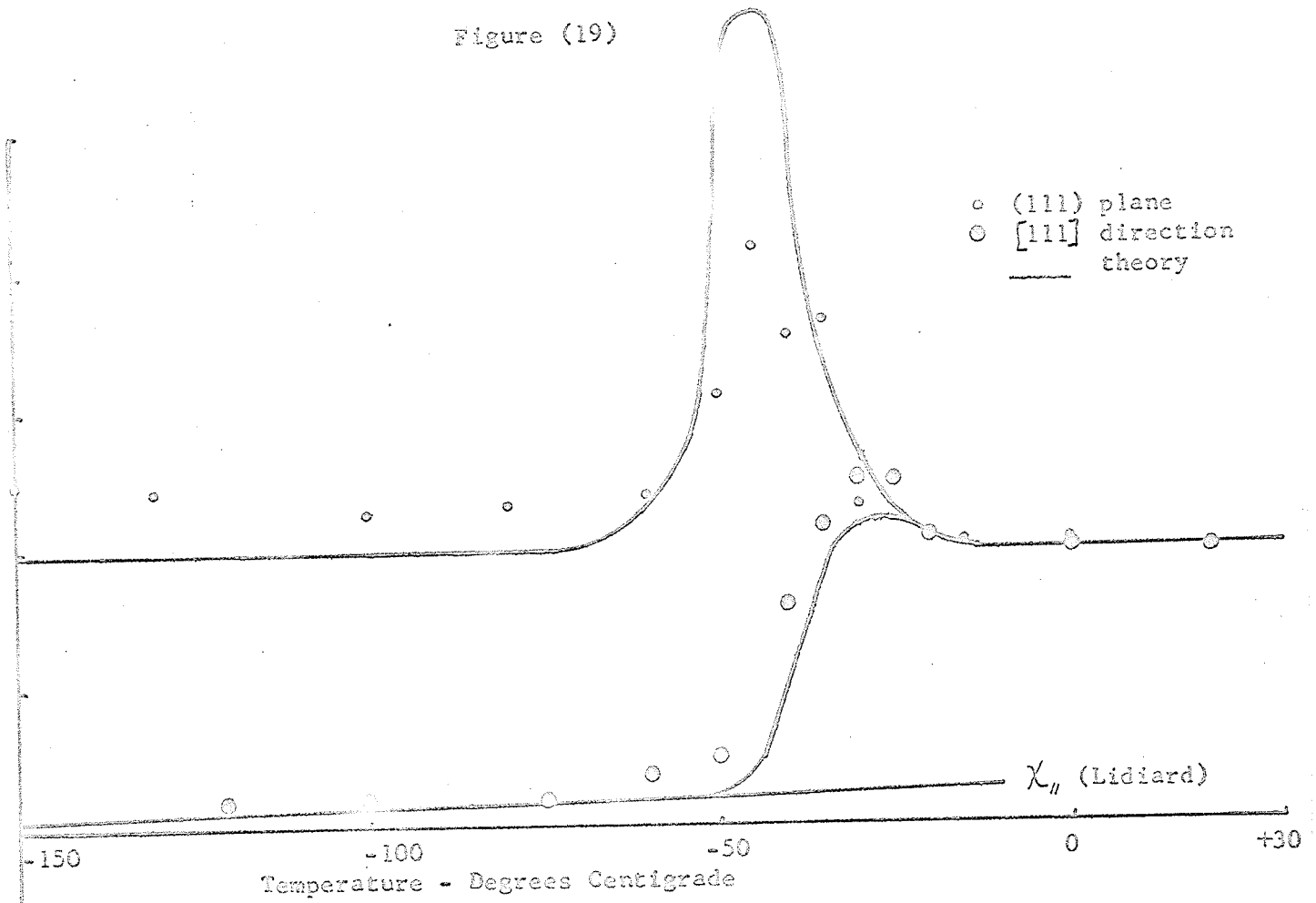
Susceptibility for 2.06% Aluminum Doped Hematite



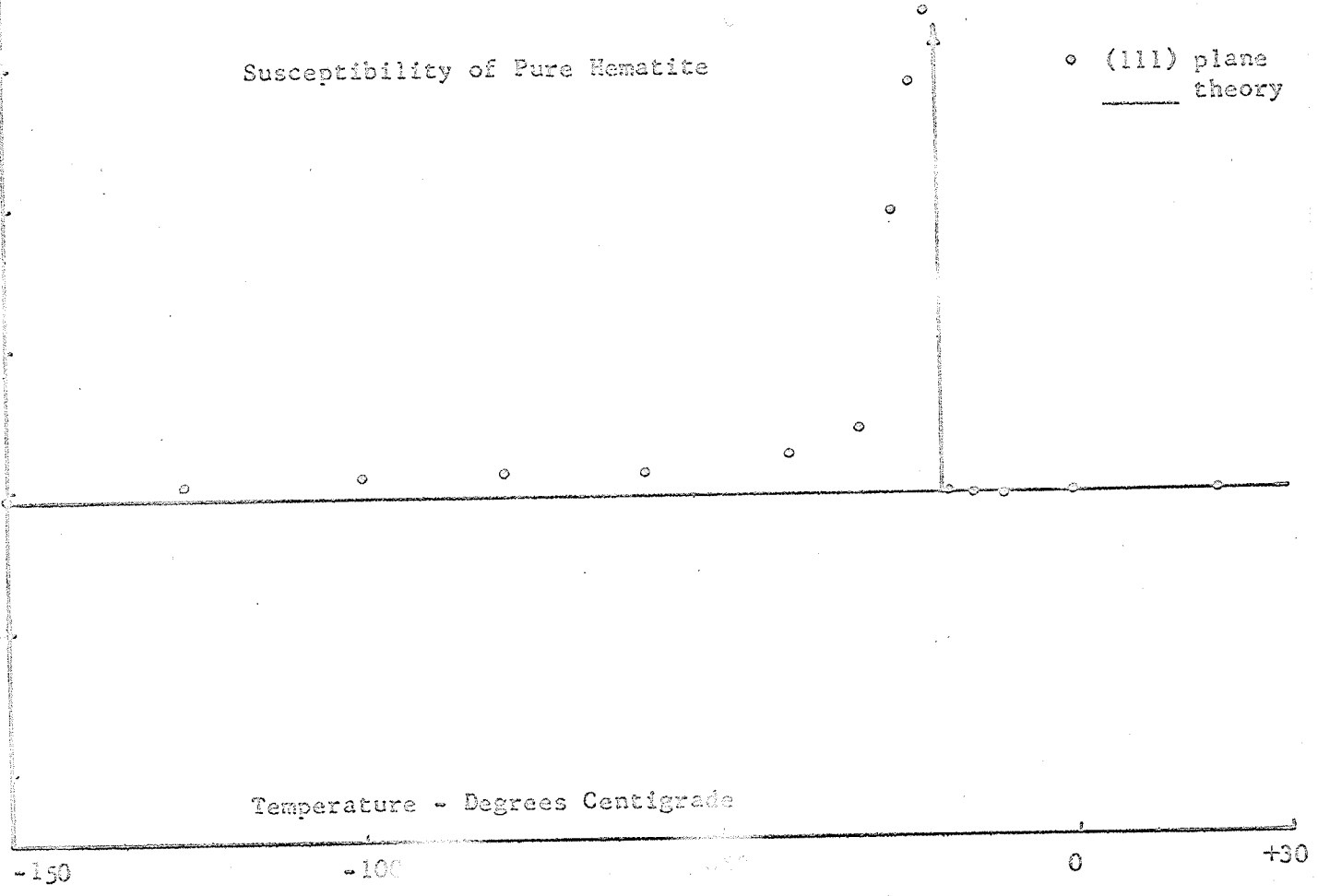
emu./gm.-oe.X10⁻⁶

Susceptibility of 1.38% Calcium Doped Hematite

Figure (19)



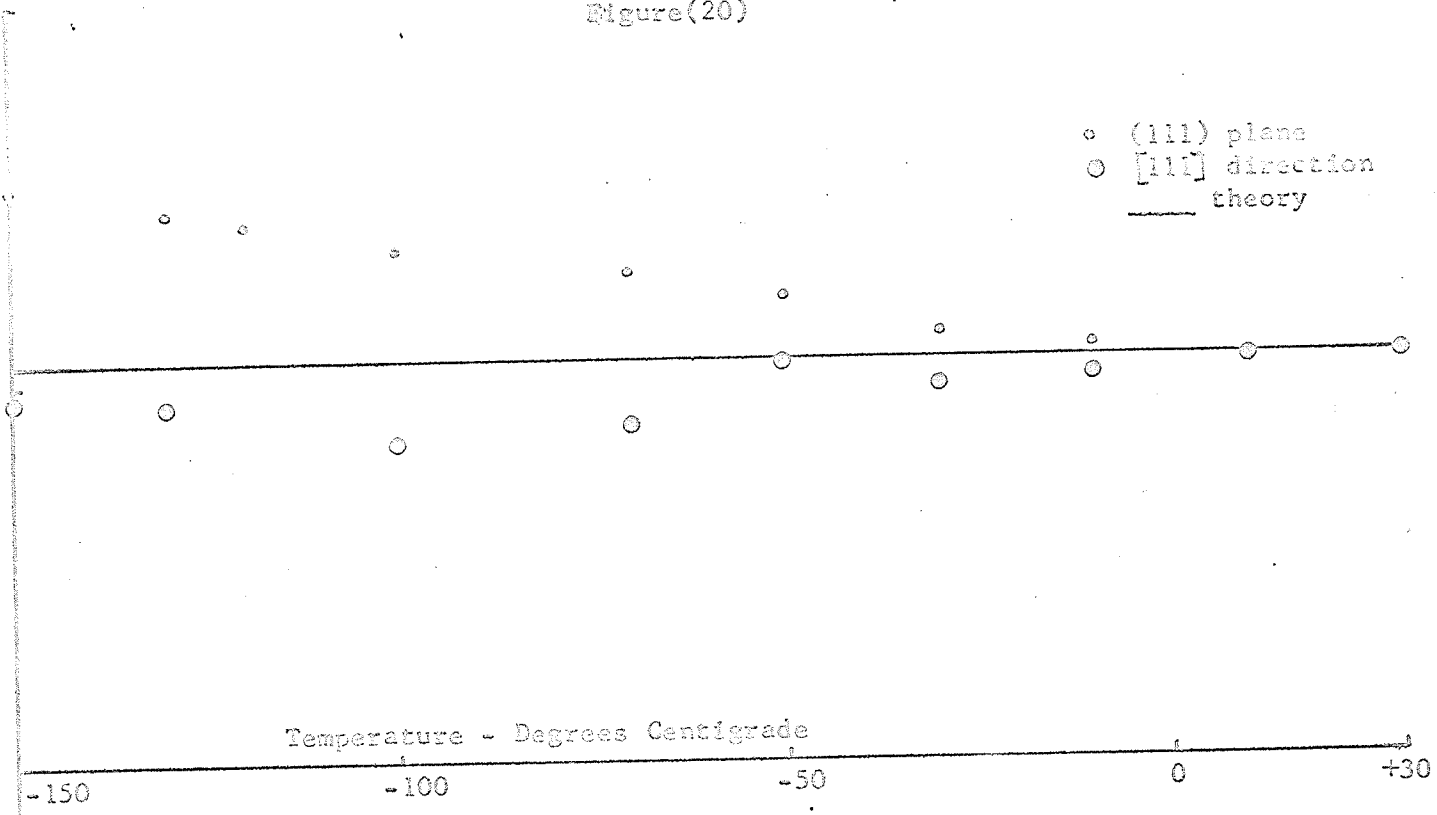
Susceptibility of Pure Hematite



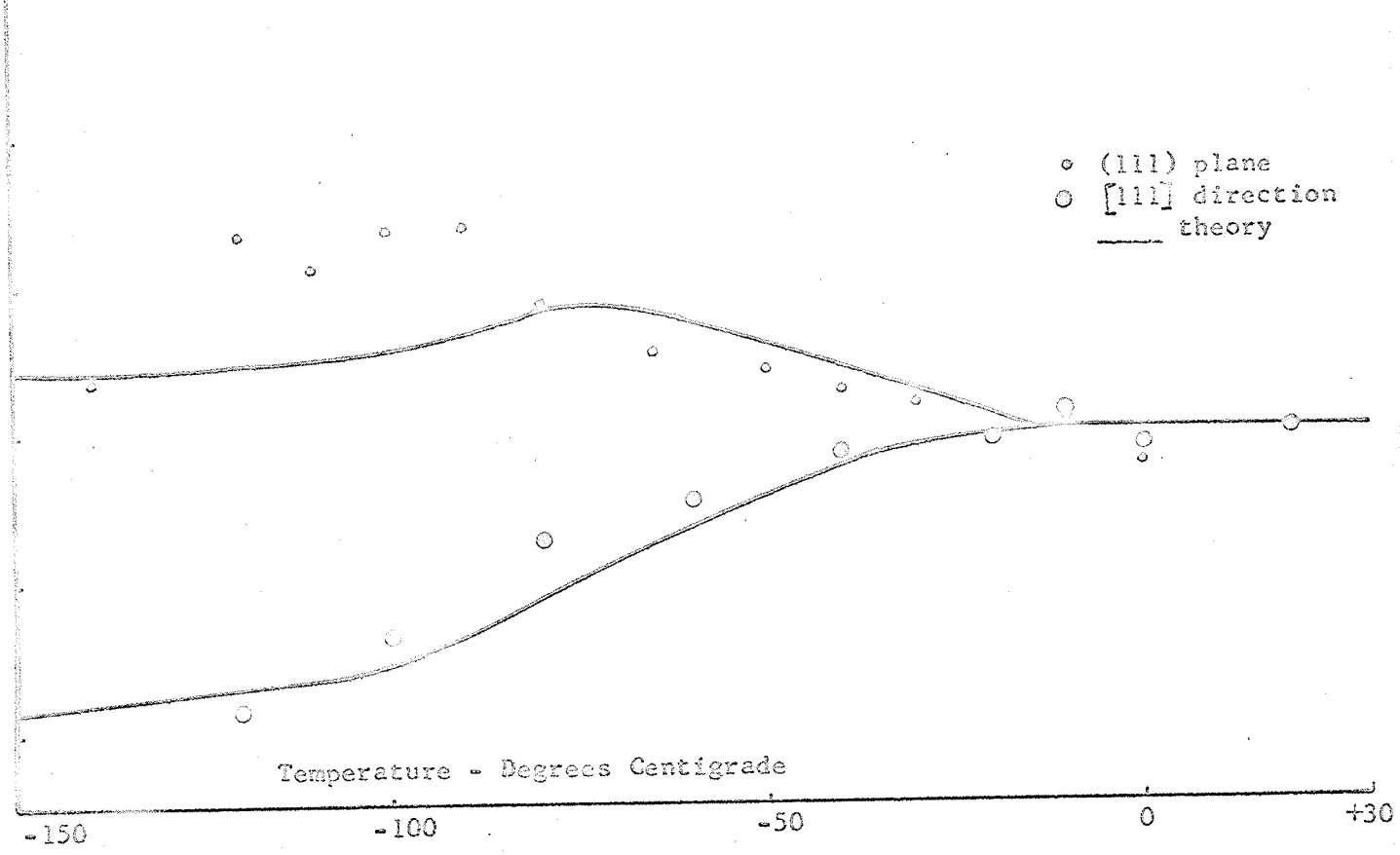
emu./gm. - $\text{cc.} \times 10^{-6}$

Susceptibility of 0.353% Titanium Doped Hematite

Figure(20)



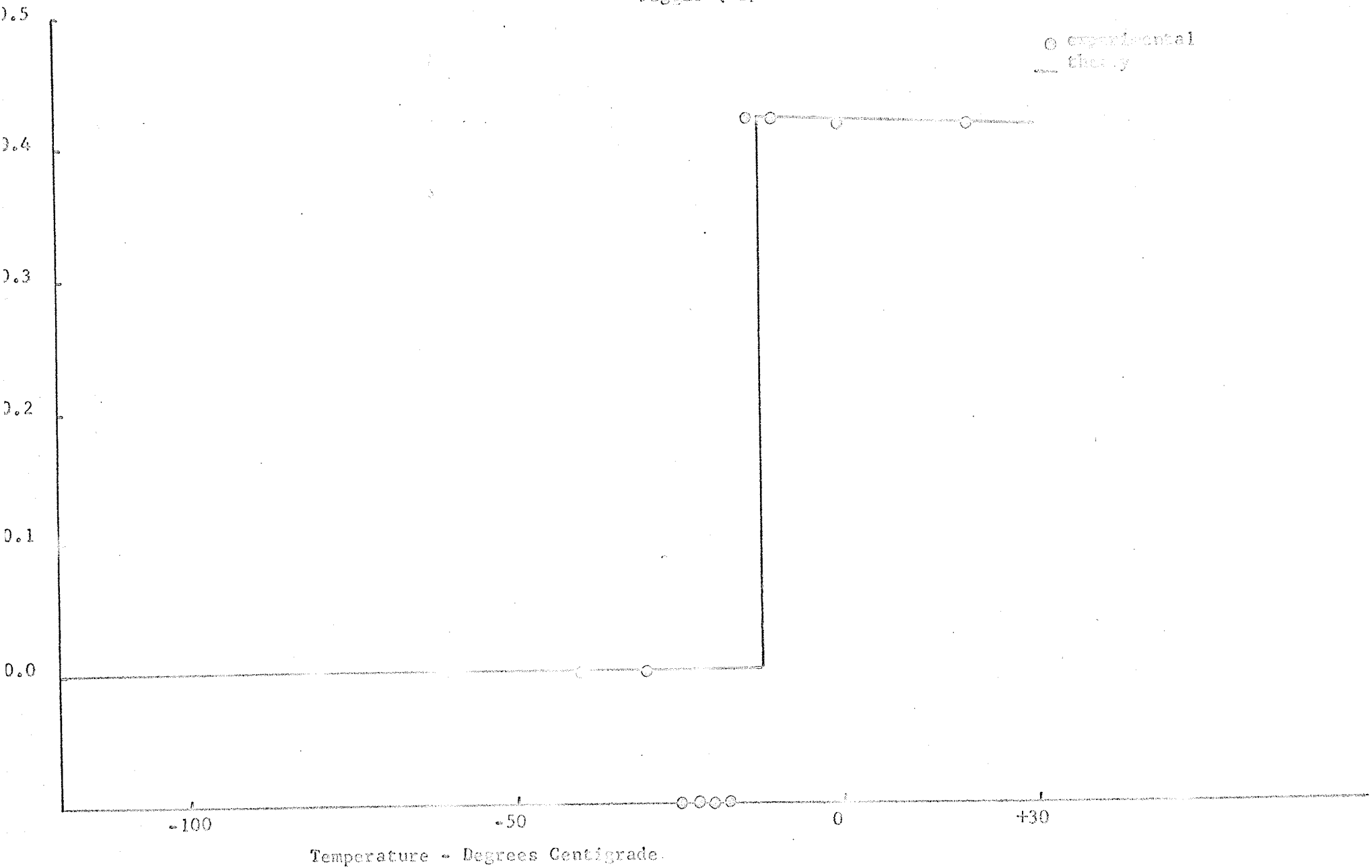
Susceptibility of 0.170% Titanium Doped Hematite



Magnetization - emu./gm.

Spontaneous Moment of Pure Hematite

Figure (21)



Spontaneous Moment of 2.06% Aluminum Doped Hematite

Figure (22)

Magnetization - emu./gm.

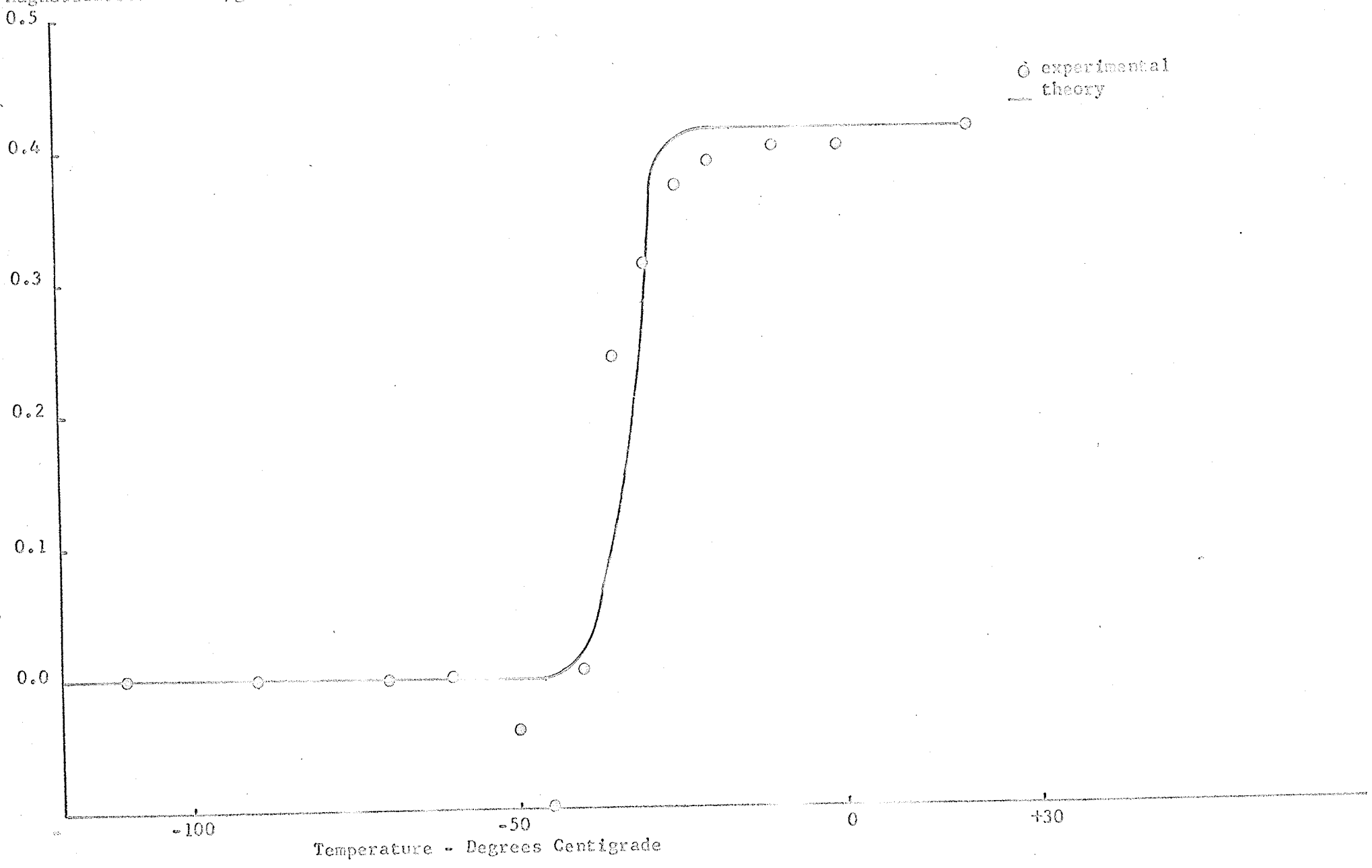
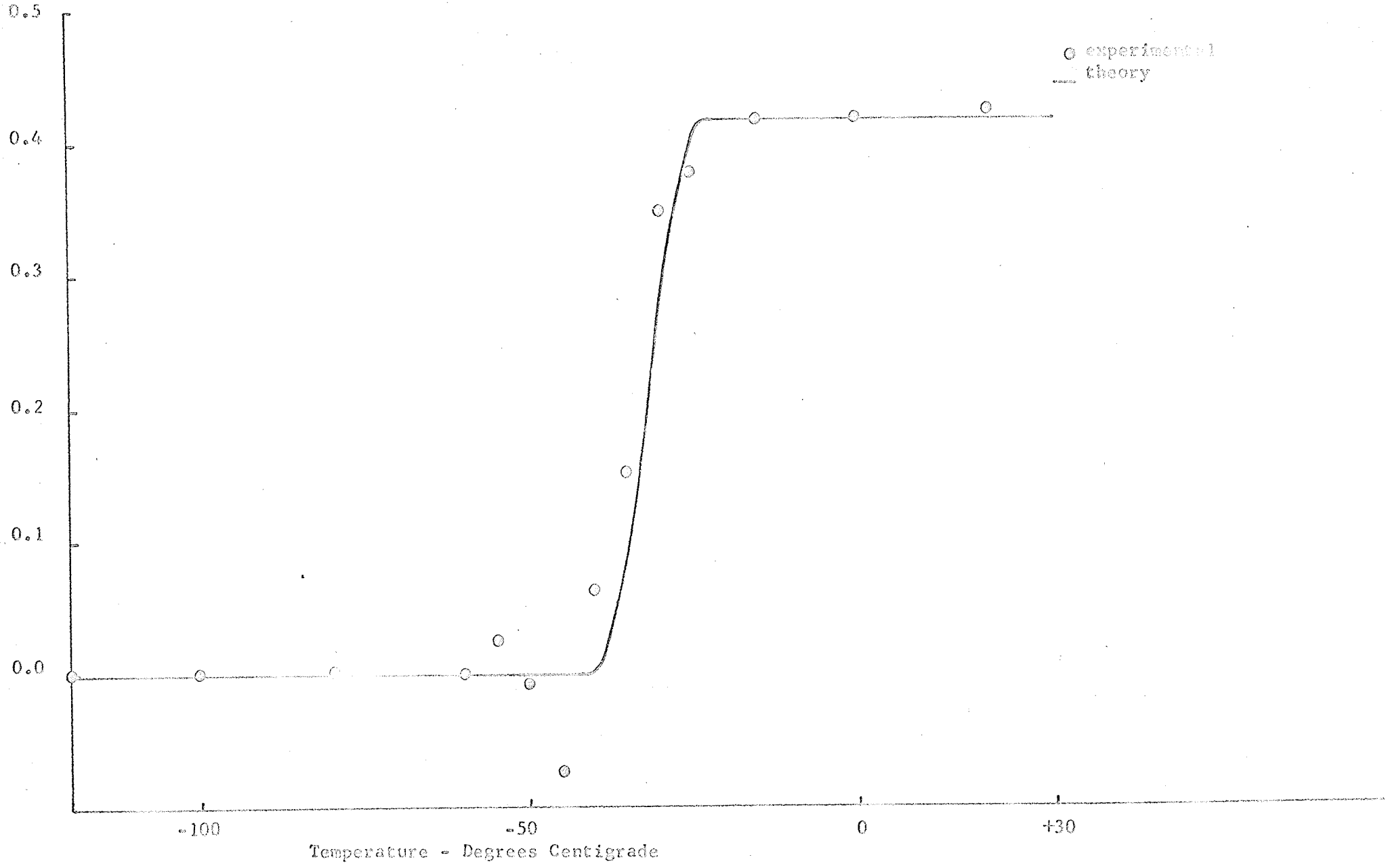


Figure (23)

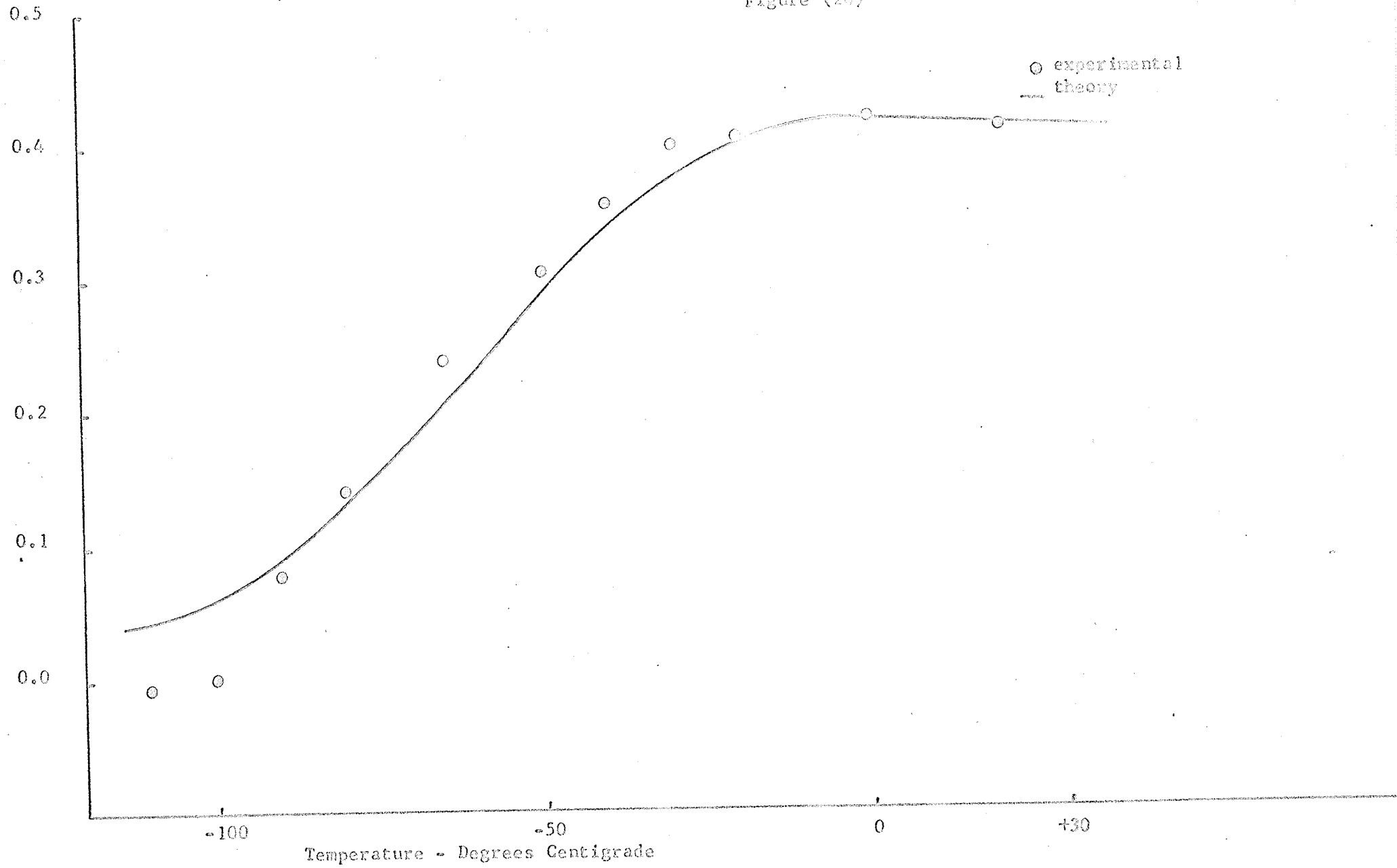
Magnetization - emu./gm.



Magnetization - emu./gm.

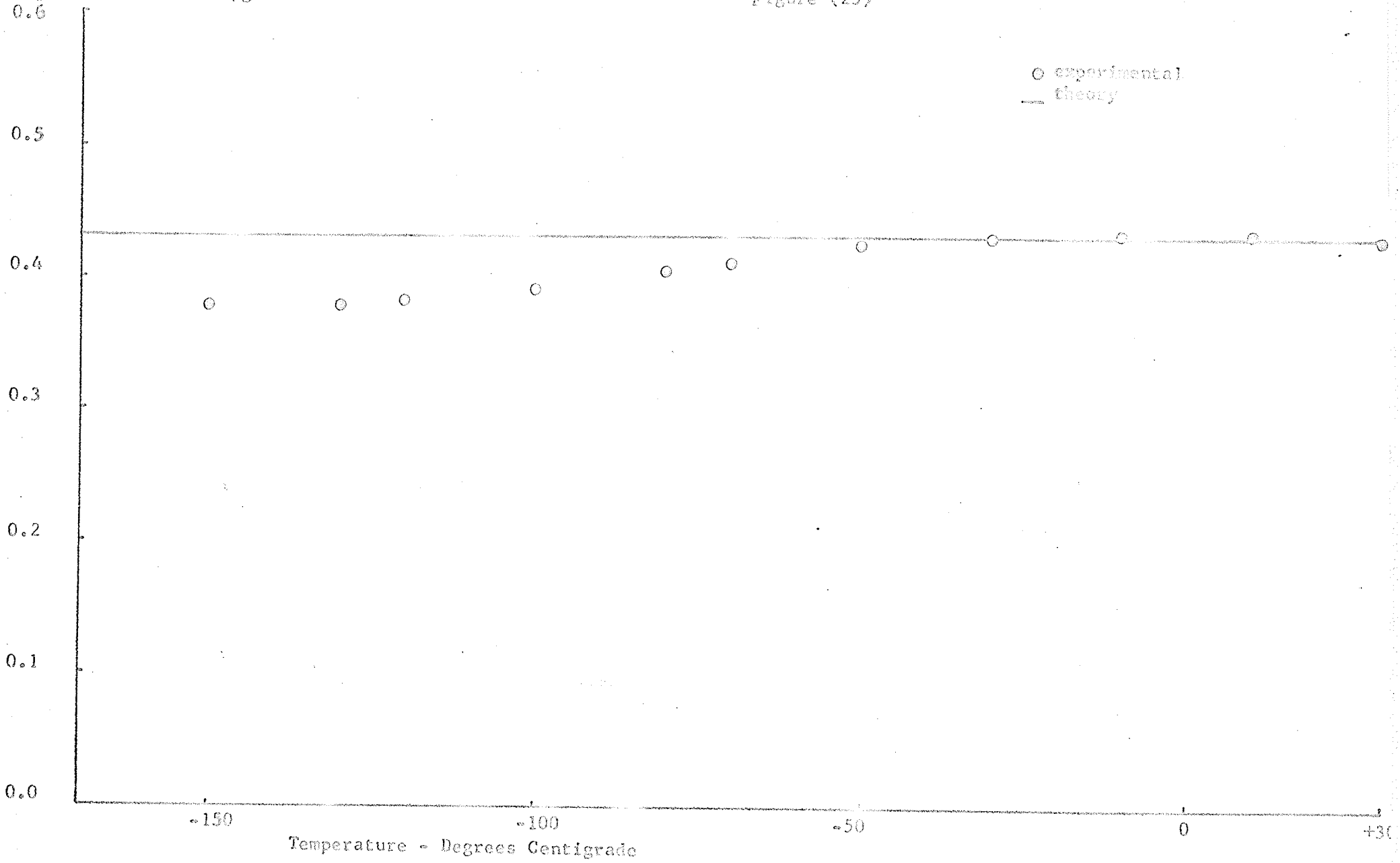
Spontaneous Moment of 0.170% Titanium Doped Hematite

Figure (26)



Magnetization - emu./gm.

Figure (25)



ization
rbitrary units

Field Induced Transitions in the Gallium Doped Crystal

Figure (26)

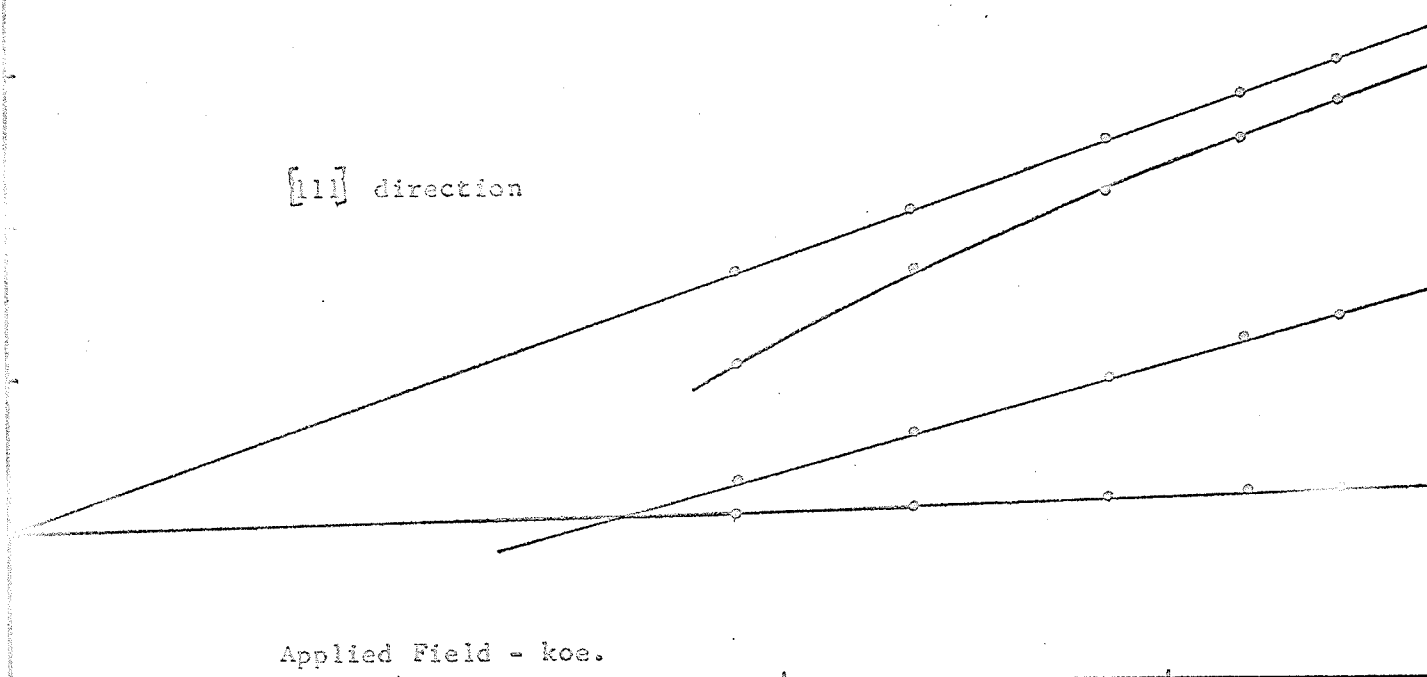
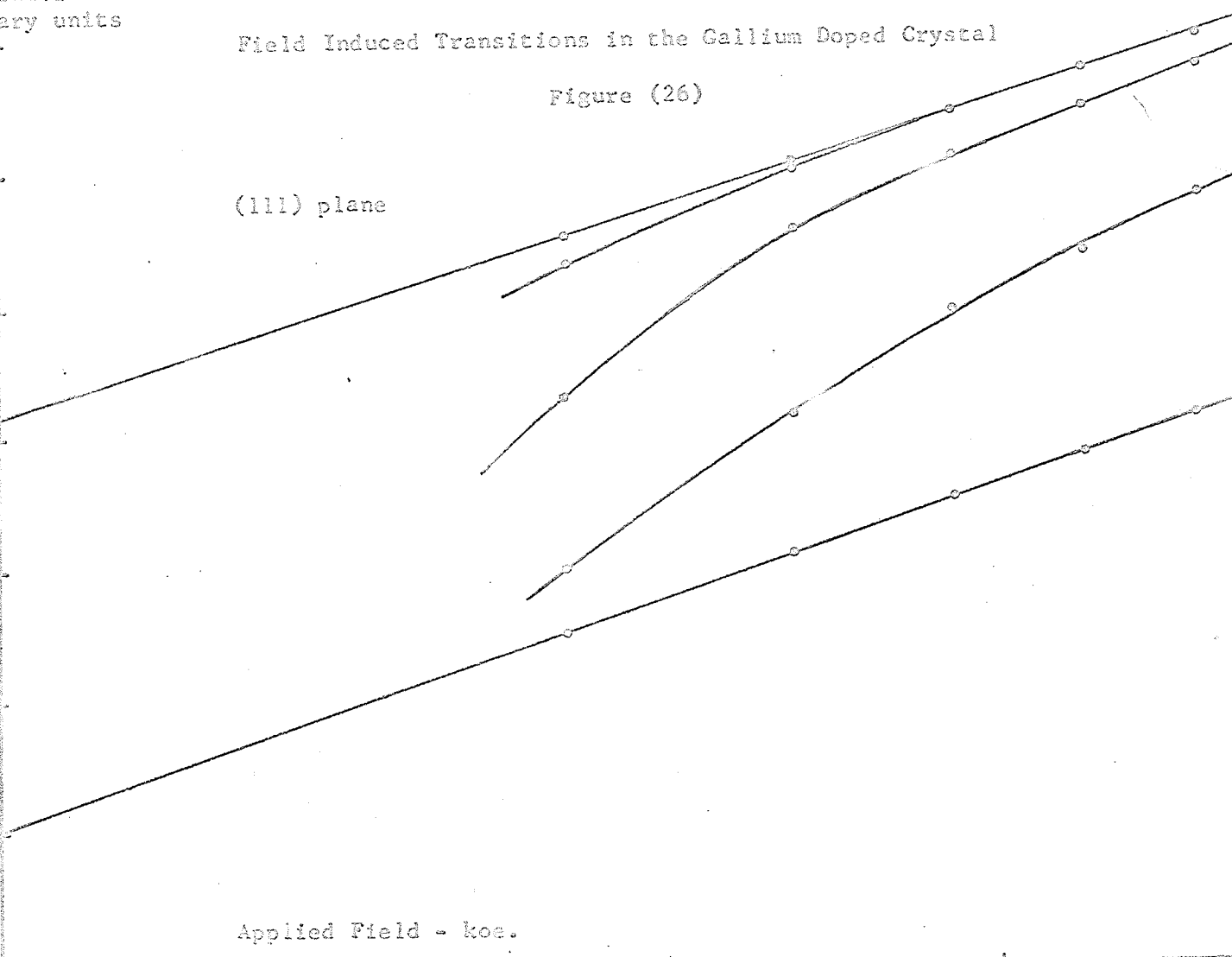
(111) plane

Applied Field - koe.



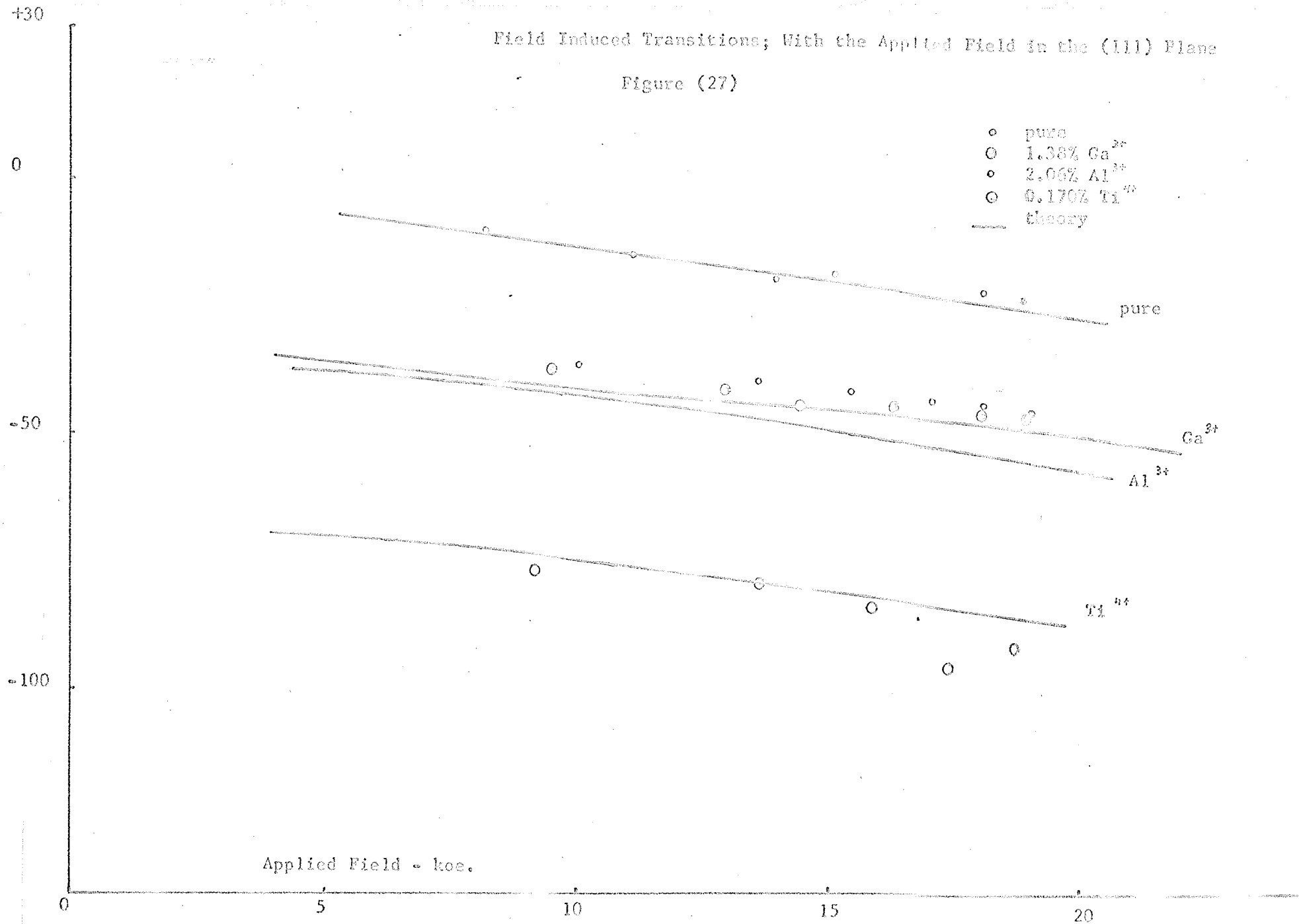
[11] direction

Applied Field - koe.



Field Induced Transitions; With the Applied Field in the (111) Plane

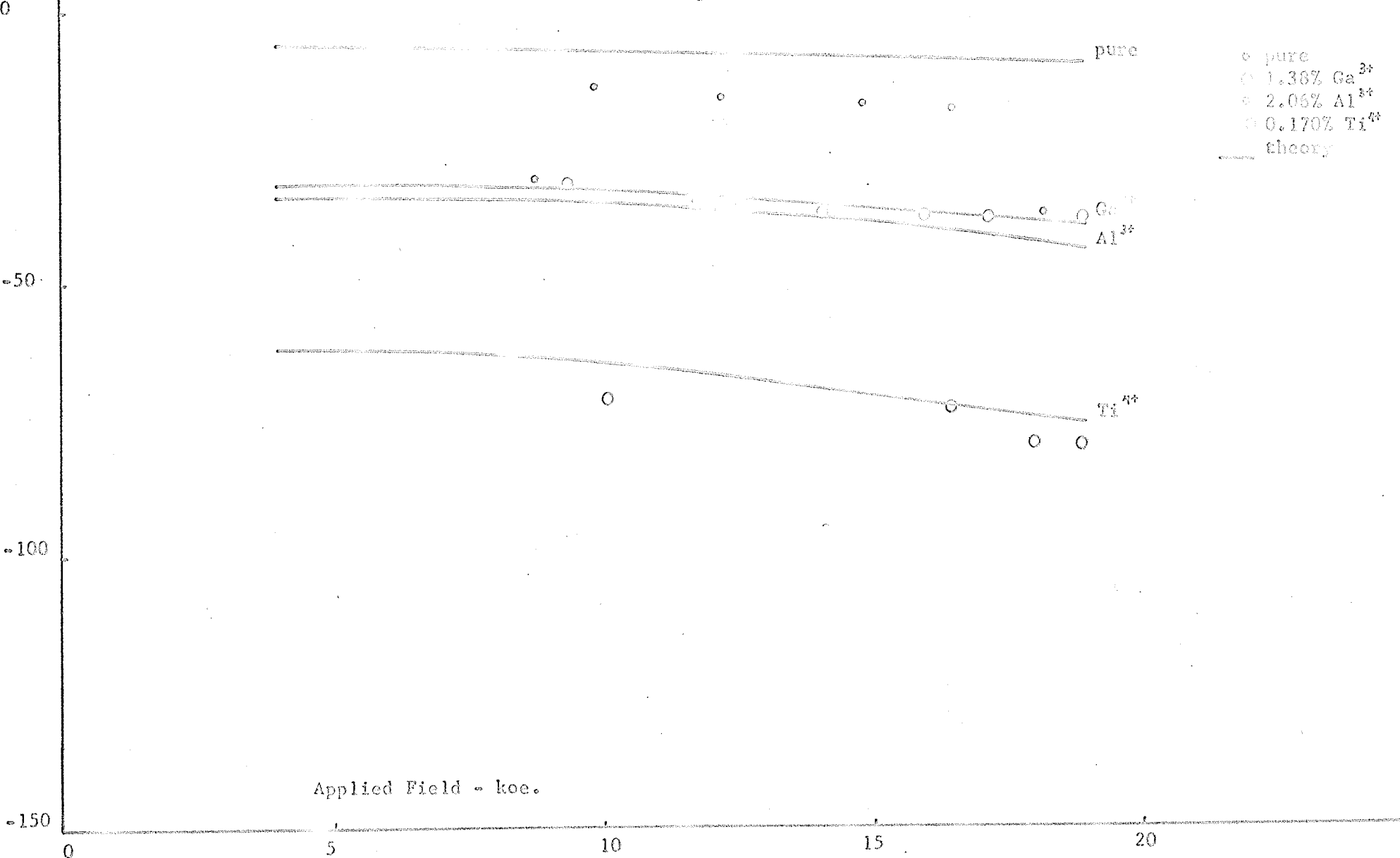
Figure (27)



Temperature - Degrees Centigrade

Field Induced Transitions; With the Applied Field in the [111] direction

Figure (28)



Applied Field - koe.

Chapter V

Discussion of Results

In the interpretation of the experimental data, considerable use has been made of the results of Chapters II and III. While the method behind these results is correct to first order; the accuracy of the factors entering into these predictions leaves something to be desired. To attain the utmost accuracy, the program used the experimentally derived constants from the spin flop data, rather than any approximate, order of magnitude theoretical estimates. Even these values are quite inaccurate, and combined with the rather limited analysis of inhomogeneity in the samples large discrepancies will occur naturally, between the experimental and theoretical curves. Indeed the microprobe analysis results for Gallium were presumed to hold, even for the Aluminum doped samples, though there is some doubt as to the accuracy of the 2.06% doping figure for the Aluminum sample. With such inaccuracies as this, the theoretical method outlined here is of mainly qualitative support to the theory that inhomogeneous doping, combined with a sharp transition in the case of constant doping, will explain the magnetic behaviour of doped hematite.

To support this statement, the graphs and table given previously are discussed with the object of seeing whether the theoretical model can explain the experimental facts, within the sufficiently wide tolerances demanded. Figure (17) is a typical magnetization curve at room temperature. It is plotted from the results of two separate trials, and thus shows the repeatability of the measurements on Hematite, as well as the shape of the magnetization curve.

Table V is a list of quantities measured at room temperature, and later used as calibrations for the temperature runs, as well as in the calculations of Chapter IV. Figures (18) to (20) are susceptibility curves in both directions as a function of temperature. The method of calculating the theoretical curves of Chapter IV was modified when it was realised that the term $\left(\frac{\partial \chi}{\partial T}\right)$ was dependent on the applied field. The effect is that the susceptibility curves, calculated at zero field will be shifted to lower temperatures by the action of the spin flop field, or the additional canting field as computed by the method of field induced transitions in Chapter IV. The theoretical curves agree fairly well with experimental data, except the theoretical curves are higher in peak magnitude of susceptibility, with slightly sharper falloff in most cases. Since all susceptibilities were evaluated for an average field of 10 koe., some of the discrepancy, especially in the case of the [111] direction, where $\chi_{//}$ depends on H^2 , could be due to a slightly different average field at which the susceptibilities were measured. These slight errors could also be due to effects not considered in the theory, such as superexchange interactions between areas of different doping, which might have an averaging or smoothing effect on the theoretical curve. The theoretical contribution from $\chi_{//}$ below the transition (Lidiard), is marked on the gallium curve. It can be seen that this contribution will be negligible, and indeed approximately equal to the noise level of the instrument.

Figures (21) to (25) are curves of the spontaneous moment, in comparison to the theory of Chapter IV. In all cases agreement is generally good except for some fine detail. The titanium sample

with a suppressed transition, appears to be starting a slow transition. This is no doubt due to regions of lighter doping in the crystal, which go through the transition at low temperatures. In small regions of the spontaneous moment curve, near the bottom part of the transition region, an approximate straight line plot of the magnetization curve would indicate a negative spontaneous moment. This effect becomes greater as the transitions become sharper and the doping decreases. For the pure samples, only extremely approximate values are possible near the transition. As this behaviour is probably caused by field induced transitions, the form of such a magnetization curve is shown in figure (26) for the gallium doped sample. In between the two transition endpoints the magnetization curves are not linear. This sample had relatively undistorted curves, since the amount of curvature increased as the impurity doping decreased. From the crude theory of field induced transitions introduced in Chapter IV, behaviour of this sort would be expected from two sources: 1, the field dependence of the term $\left(\frac{\partial R}{\partial \frac{T_M}{T_N}}\right)$, or the slope of the spontaneous moment curve: an applied field shifts the point at which the slope is evaluated down the curve, the effect being largest for a field in the (111) plane 2, the field dependence of the term $\left(\frac{\partial \Delta E}{\partial H}\right)$, which is only important in the $[111]$ direction; and gives the predicted partly parabolic dependence of $\chi([111])$ on applied field. For both directions the experimental curves are linear for high fields, tapering asymptotically to zero past a certain point. Although this would seem to disprove the theories of 30 and 31 it agrees qualitatively with expectations from the above terms. The experimental points on magnetization curves

in the transition region were too inaccurate, too few, and over too small a range of H to make a meaningful comparison with a calculated curve. As another minor irregularity, the pure sample must still contain some impurity ions, or it would have a transition sharpness limited only by the response time of the instrument, and an infinite spike in the susceptibility curve at the transition temperature.

The final graphs are an illustration of how the spin flop energy, and the additional canting energy due to an applied field, can shift the observed and predicted transition temperatures. Again agreement is reasonable if not exact.

In conclusion, it is felt that the method pursued here, explains the greater part of the magnetization data gathered on Hematite. Greater accuracy in the anisotropy calculations will be required before all difficulties at the transition can be eliminated. It is reasonable to say, that the experimental evidence supports this work at its present state.

Bibliography

1. L. Pauling and S. B. Hendricks, J. Amer. Chem. Soc. 47, 781(1925)
2. T. Zoltai and R. Blake, Private Communication
3. J. O. Artman, J. C. Murphy, and S. Foner, Phys. Rev. 138, A912(1965)
4. C. G. Shull, W. A. Strauser, and E. O. Wollan, Phys. Rev. 83, 333(1951)
5. P. W. Anderson, Phys. Rev. 79, 350(1950)
6. M. A. Gilleo, Phys. Rev. 109, 777(1958)
7. Toru Moriya, Phys. Rev. 120, 91(1960)
8. S. Chikazumi, "Physics of Magnetism" Wiley, p 153(1964)
9. M. Tachiki and T. Nagamiya, J. Phys. Soc. Japan 13, 452(1958)
10. Kei Yosida, Progress Theoretical Physics 6, 691(1951)
11. P. J. Besser, A. H. Morrish, and C. W. Searle, Phys. Rev. 153, 632(1967)
12. M. H. L. Pryce, Phys. Rev. 80, 1107(1950)
13. H. F. Symmet and G. S. Bogle, Proc. Phys. Soc. (LONDON), 79, 468(1961)
14. R. R. Sharma, T. P. Das, and R. Orbach, Phys. Rev. 149, 257(1966)
15. R. R. Sharma, T. P. Das, and R. Orbach, Phys. Rev. 155, 338(1967)
16. P. W. Anderson, "Magnetism Vol. I", Academic Press (1963)
17. R. C. Ohlman and M. Tinkham, Phys. Rev. 123, 425(1961)
18. W. Low, "Paramagnetic Resonance in Solids", Academic Press (1960)
19. W. A. Yagar, J. K. Galt, and F. R. Merritt, Phys. Rev. 99, 1788(1955)
20. D. O. Smith, Phys. Rev. 102, 959(1956)
21. M. Tinkham, Proc. Royal Soc. (LONDON), A236, 549(1956)
22. K. W. H. Stevens, "Magnetism II", Academic Press (1963)
23. R. E. Trees, Phys. Rev. 82, 683(1951)
24. C. W. Searle and A. H. Morrish, J. Applied Physics, 37, 1141(1966)
25. S. K. Banerjee, W. O'Reilly, T. C. Gibb, N. N. Greenwood, J. Phys. Chem. of Solids, 28, 1323(1967)

26. P. W. Anderson and H. Hasegawa, Phys. Rev. 100, 675(1956)
27. P. G. DeGennes, Phys. Rev. 118, 141(1960)
28. A. B. Lidiard, Rept. Prog. Phys. 25, 441(1962)
29. A. M. Morrish, "The Properties of Magnetic Materials", Wiley (1965)
30. T. Kaneko and S. Abe, J. Phys. Soc. Japan 20, 2001(1965)
31. G. Cinader and S. Shtrikman, Solid State Communications 4, 459(1966)
32. S. Wang and C. W. Searle, Unpublished Data
33. J. Kanamori, "Magnetism I", Wiley (1963)
34. A. A. Missetich and R. E. Watson, Phys. Rev. 143, 335(1966)
35. J. Yamashita and J. Kondo, Phys. Rev. 109, 730(1958)
36. Toru Moriya, Phys. Rev. 117, 635(1959)
37. J. D. Axe and G. Burns, Phys. Rev. 152, 331(1966)
38. G. A. Acket and J. Volger, Physica 32, 1543(1966)
39. H. J. Van Daal and A. J. Bosman, Phys. Rev. 158, 736(1967)
40. Kei Yosida, Phys. Rev. 147, 223(1966)
41. S. Foner, Rev. Sci. Ins. 30, 548(1959)
42. K. Yosida and M. Tachiki, Prog. Theo. Phys. 17, 331(1957)
43. I. Dzialoshinski, J. Phys. Chem. of Solids, 4, 421(1955)